Supporting Information for

Force-Dependent Multicolor Mechanochromism from a Single Mechanophore

Molly E. McFadden and Maxwell J. Robb*

Division of Chemistry and Chemical Engineering, California Institute of Technology, Pasadena, California 91125, United States

*To whom correspondence should be addressed. E-mail: mrobb@caltech.edu

Table of Contents

I. General Experimental Details

Reagents from commercial sources were used without further purification unless otherwise stated. Methyl acrylate was passed through a short plug of basic alumina to remove inhibitor immediately prior to use. Dry THF was obtained from a Pure Process Technology solvent purification system. All reactions were performed under a N_2 or argon atmosphere unless specified otherwise. Column chromatography was performed on a Biotage Isolera system using SiliCycle SiliaSep HP flash cartridges.

NMR spectra were recorded using a 400 MHz Bruker Avance III HD with Prodigy Cryoprobe, a 400 MHz Bruker Avance Neo, or Varian Inova 500 or 600 MHz spectrometers. All ^{1}H NMR spectra are reported in δ units, parts per million (ppm), and were measured relative to the signals for residual $CHCl_3$ (7.26 ppm) or CH_2Cl_2 (5.32 ppm) in deuterated solvent. All ^{13}C NMR spectra were measured in deuterated solvents and are reported in ppm relative to the signals for $^{13}CDCl_3$ (77.16 ppm) or $^{13}CD_2Cl_2$ (54.00 ppm). Multiplicity and qualifier abbreviations are as follows: s = singlet, d = doublet, m = multiplet, br = broad, app = apparent. Peaks were assigned on the basis of 2D NMR experiments (COSY, HSQC, and HMBC). $^{1}H–^{19}F$ coupling constants were determined from $^{1}H\{^{19}F\}$ NMR spectra acquired on a 400 MHz Bruker Avance Neo spectrometer.

High resolution mass spectra (HRMS) were obtained from an Agilent 6200 series time-of-flight mass spectrometer equipped with an Agilent G1978A multimode source (ESI+).

Analytical gel permeation chromatography (GPC) was performed using an Agilent 1260 series pump equipped with two Agilent PLgel MIXED-B columns (7.5 x 300 mm), an Agilent 1200 series diode array detector, a Wyatt 18-angle DAWN HELEOS light scattering detector, and a Optilab rEX differential refractive index detector. The mobile phase was THF at a flow rate of 1 mL/min. Molecular weights and molecular weight distributions were calculated by light scattering using a dn/dc value of 0.062 mL/g (25 °C) for poly(methyl acrylate). Preparative HPLC was performed on a Agilent 1100 Series apparatus using three Eclipse XDB-C18 9.4 x 250 mm columns in series.

UV-Vis absorption spectra were recorded on a Thermo Scientific Evolution 220 spectrometer.

Ultrasound experiments were performed using a Vibra Cell 505 liquid processor equipped with a 0.5-inch diameter solid probe (part #630-0217), sonochemical adapter (part #830-00014), and a Suslick reaction vessel made by the Caltech glass shop (analogous to vessel #830-00014 from Sonics and Materials). UV irradiation was performed using a Philips PL-S 9W/01/2P UVB bulb with a narrow emission of 305–315 nm and a peak at 311 nm under ambient conditions unless indicated otherwise. A Thermo Scientific EK45 Immersion Cooler (part #3281452) was used to maintain a constant temperature bath for sonication and photoirradiation experiments. Polymer solutions were continuously sampled for UV-vis analysis using a Cole Parmer Masterflex L/S pump system (item #EW-77912-10) composed of an L/S pump head (part #77390-00) and L/S precision variable speed drive (part #07528-20) using 4x6 mm PTFE tubing (part #77390-60) and a quartz flow-through cell (Starna, part #583.4-Q-10/Z8.5), which was connected using M6-threaded PTFE tubing (Starna, part #M6-SET).

II. Supplementary Figures

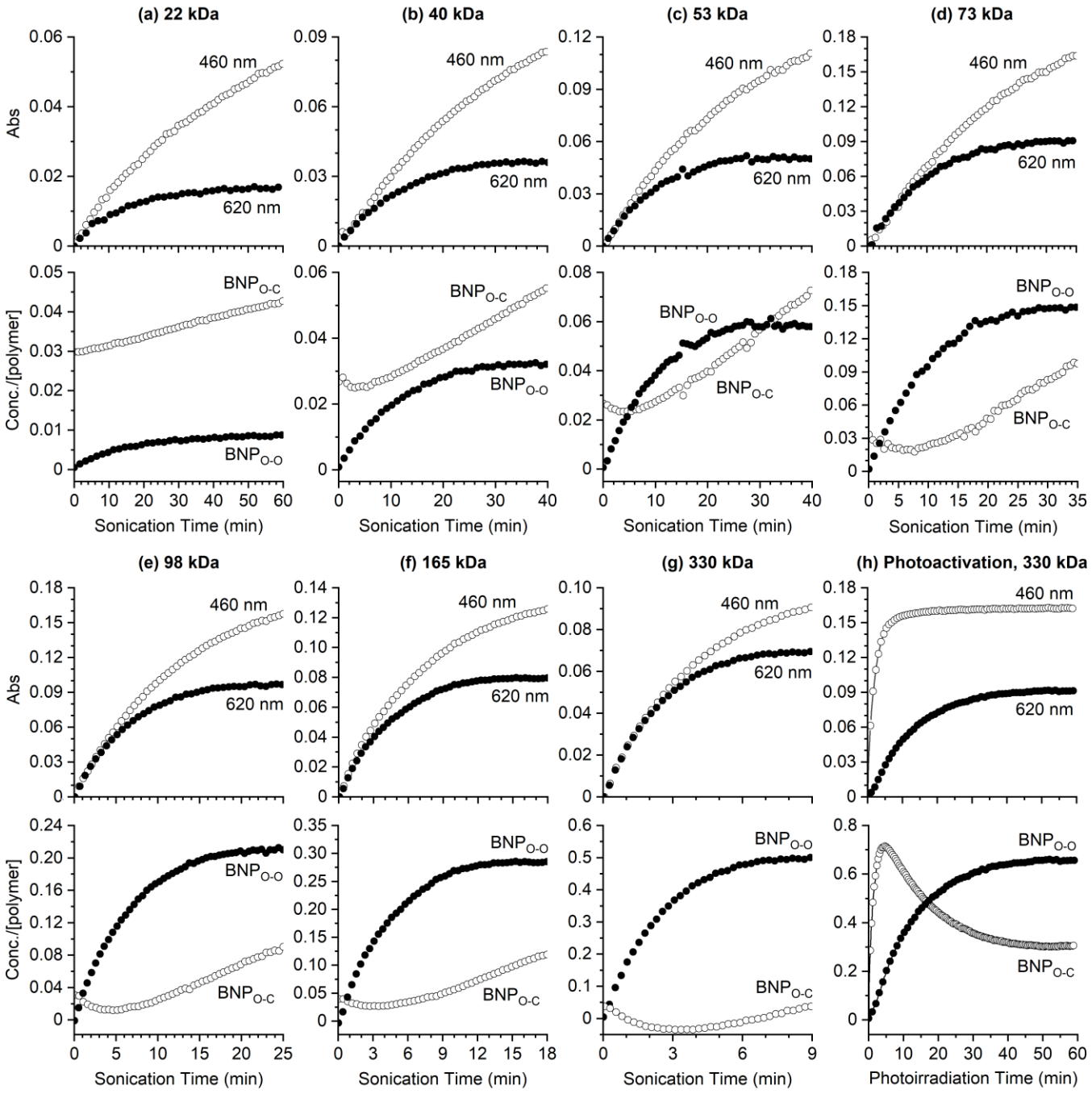

Figure S1. (a–g) Representative absorbance (*top*) and concentration (*bottom*) data for the mechanochemical activation of all polymers. (h) Absorbance and concentration data collected during photochemical activation of **BNP-PMA$_{330}$** with 311 nm UV light. Concentrations of merocyanine species BNP$_{O-C}$ and BNP$_{O-O}$ were determined from the absorption data using estimated extinction coefficients (see section VII for details). All reactions were conducted at −45 °C with 2 mg/mL polymer in THF. Concentrations of BNP$_{O-C}$ and BNP$_{O-O}$ are scaled to the total molar concentration of polymer in solution.

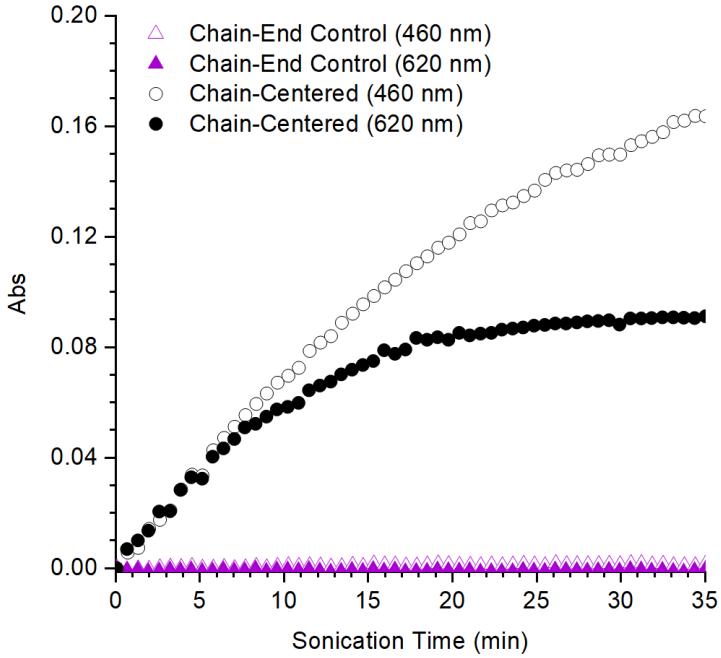

Figure S2. Absorbance monitored at 460 nm and 620 nm during continuous ultrasonication (−45 °C, 2 mg/mL in THF) of a 73 kDa chain-centered polymer (**BNP-PMA$_{73}$**) and a 71 kDa chain-end functional control polymer (**BNP-PMA$_{Control}$**) . In contrast to the polymer with a chain-centered BNP unit, no changes in the absorbance at 460 nm or 620 nm are observed for the control polymer containing a BNP unit at the chain-end, confirming that mechanical force is responsible for the observed activation of the BNP mechanophore during ultrasonication.

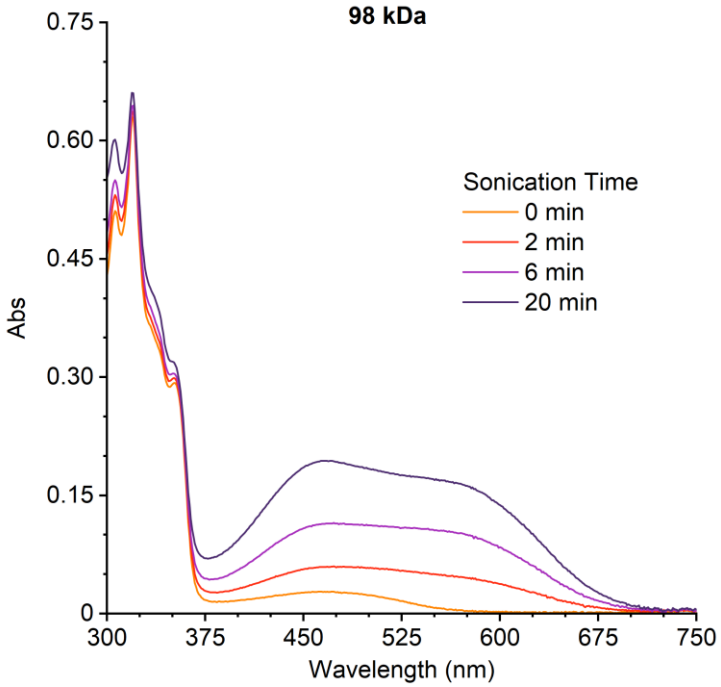

Figure S3. Representative absorption spectra in the wavelength range 300–750 nm of **BNP-PMA$_{98}$** subjected to ultrasound-induced mechanochemical activation for varying amounts of time (−45 °C, 2 mg/mL polymer in THF).

Figure S4. Photographs of polymer solutions (2 mg/mL in THF) subjected to ultrasound-induced mechanochemical activation. (*left*) **BNP-PMA$_{40}$** after 30 min of sonication, and (*right*) **BNP-PMA$_{330}$** after 9 min of sonication. Immediately after cessation of sonication, the reaction vessel was removed from the cooling bath, sprayed with isopropanol to prevent water condensation, the vessel was illuminated with a fluorescent lamp and immediately photographed. Images were acquired in RAW format to preserve color information.

III. Synthetic Details

Scheme S1. Synthesis of bis-naphthopyran initiator **1**.

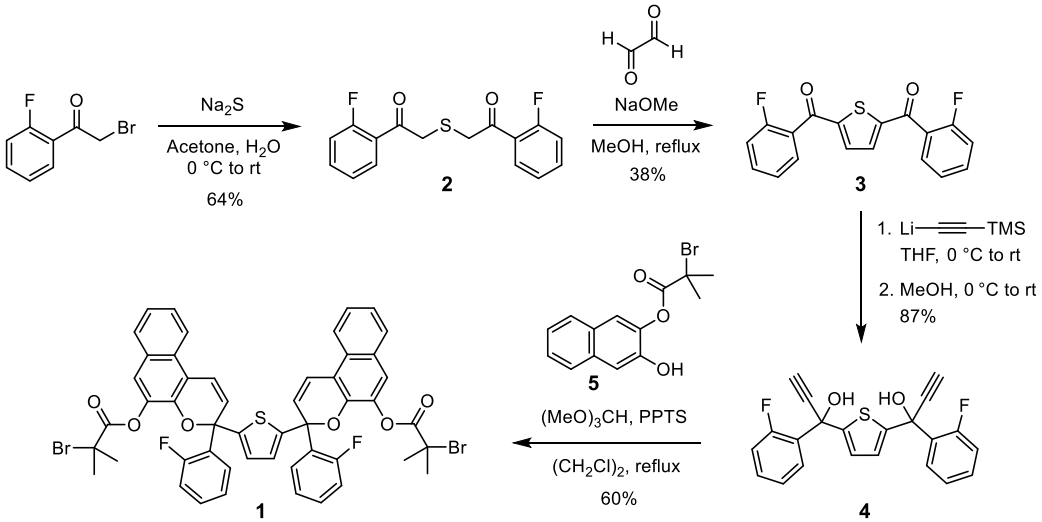

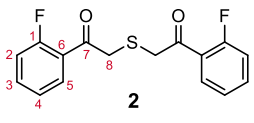

2

2,2′-Thiobis(1-(2-fluorophenyl)ethan-1-one) (2). A round bottom flask equipped with a stir bar was charged with 2-bromo-2′-fluoroacetophenone (13.6 g, 62.3 mmol) dissolved in acetone (150 mL). The solution was cooled to 0 °C in an ice bath followed by the dropwise addition of sodium sulfide nonahydrate (7.53 g, 31.4 mmol) dissolved in DI water (17 mL). The reaction was allowed to warm to room temperature and stirred for 25 h. The solution was concentrated under reduced pressure and the aqueous solution was extracted into dichloromethane, dried over $MgSO_4$, filtered, and concentrated. The crude material was purified by column chromatography on silica gel (30% EtOAc/hexanes) to provide the title compound as pale-yellow crystals (6.16 g, 64%).

TLC (20% EtOAC/hexanes): R_f = 0.43

^{1}H NMR (500 MHz, CD_2Cl_2) δ: 3.92 (d, J_{HF} = 2.4 Hz, 4H, C_8), 7.16 (ddd, J_{HF} = 11.4 Hz, J_{HH} = 8.4 Hz, 1.1 Hz, 2H, C_2), 7.26 (ddd, J_{HH} = 7.8, 7.3, 1.1 Hz, 2H, C_4), 7.57 (dddd, J_{HF} = 5.1 Hz, J_{HH} = 8.3, 7.1, 1.9 Hz, 2H, C_3), 7.88 (ddd, J_{HF} = 7.6 Hz, J_{HH} = 7.6, 1.9 Hz, 2H, C_5).

^{13}C{^{1}H} NMR (101 MHz, $CDCl_3$) δ: 42.0 (d, J_{CF} = 8.3 Hz, C_8), 116.8 (d, J_{CF} = 23.9 Hz, C_2), 124.1 (d, J_{CF} = 12.6 Hz, C_6), 124.8 (d, J_{CF} = 3.3 Hz, C_4), 131.4 (d, J_{CF} = 2.5 Hz, C_5), 135.3 (d, J_{CF} = 9.2 Hz, C_3), 161.9 (d, J_{CF} = 254.6 Hz, C_1), 192.0 (d, J_{CF} = 4.6 Hz, C_7).

HRMS (ESI, *m/z*): calcd for $[C_{16}H_{13}F_2O_2S]^+$ $(M+H)^+$, 307.0599; found, 307.0604.

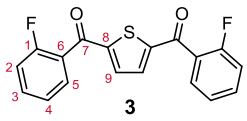

3

2,5-Di(*o*-fluorobenzoyl)thiophene (3). A flame-dried round bottom flask equipped with a condenser and stir bar was charged with 2,3-dihydroxy-1,4-dioxane (0.922 g, 7.68 mmol) and evacuated/backfilled with nitrogen (3x). Anhydrous methanol (50 mL) was added via syringe and the mixture was heated to reflux for 1.5 h to generate glyoxal. In a separate flame-dried round bottom flask equipped with a condenser and stir bar, sodium metal (340 mg, 14.8 mmol) was dissolved in anhydrous methanol (15 mL) under nitrogen at 0 °C in an ice bath to form sodium methoxide. Compound **2** (3.795 g, 12.31 mmol) was dissolved in anhydrous dichloromethane (15 mL) under nitrogen and transferred via syringe to the warm glyoxal solution, followed by the dropwise addition of the sodium methoxide solution via syringe (the solution turned orange, then yellow, then dark green). The reaction mixture was returned to reflux (turning dark red) and stirred for 16 h. The reaction was cooled to room temperature, concentrated under reduced pressure, and dissolved in EtOAc (100 mL). The organic layer was washed with 1 M aqueous HCl (100 mL), distilled water (100 mL), 10% aqueous $NaHCO_3$ (100 mL), 2 M aqueous NaOH (100 mL), and brine (100 mL). The organic layer was dried over $MgSO_4$, filtered, and concentrated under reduced pressure. The crude material was purified by column chromatography on silica gel (10–40% EtOAc/hexanes) and subsequently recrystallized from EtOAc/hexanes to provide the title compound as white needles (1.52 g, 38%).

TLC (20% EtOAc/hexanes): R_f = 0.35

^{1}H NMR (500 MHz, $CDCl_3$) δ: 7.21 (ddd, J_{HF} = 9.6 Hz, J_{HH} = 8.3, 1.0 Hz, 2H, C_2), 7.29 (ddd, J_{HH} = 7.5 Hz, 7.5, 1.0 Hz, 2H, C_4), 7.54–7.59 (m, 4H, C_3 and C_9), 7.61 (ddd, J_{HF} = 6.9 Hz, J_{HH} = 7.7, 1.8 Hz, 2H, C_5).

$^{13}C\{^{1}H\}$ NMR (101 MHz, $CDCl_3$) δ: 116.8 (d, J_{CF} = 21.5 Hz, C_2), 124.6 (d, J_{CF} = 3.7 Hz, C_4), 126.4 (d, J_{CF} = 14.5 Hz, C_6), 130.5 (d, J_{CF} = 2.5 Hz, C_5), 133.9 (d, J_{CF} = 8.4 Hz, C_3), 134.4 (d, J_{CF} = 2.9 Hz, C_9), 149.8 (C_8), 159.9 (d, J_{CF} = 253.5 Hz, C_1), 185.4 (C_7).

HRMS (ESI, *m/z*): calcd for $[C_{18}H_{11}F_2O_2S]^+$ $(M+H)^+$, 329.0442; found, 329.0444.

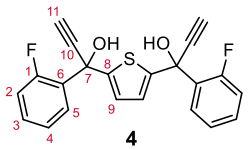

4

2,5-Di[hydroxyl-1-(*o*-fluorophenyl)-prop-2-ynyl]thiophene (4). A flame-dried round bottom flask equipped with a stir bar under nitrogen was charged with anhydrous THF (4 mL) and ethynyltrimethylsilane (0.160 mL, 1.15 mmol). The solution was cooled to 0 °C in an ice bath and n-butyllithium (2.5 M in hexanes, 0.450 mL, 1.13 mmol) was added dropwise via syringe. After 1 h, compound **3** (131 mg, 0.399 mmol) dissolved in anhydrous THF (1 mL) was added to the reaction mixture and it was allowed to warm to room temperature. After 21 h, the solution was cooled to 0 °C in an ice bath. Methanol (3 mL) was added to the solution via syringe and the reaction mixture was allowed to warm to room temperature and stirred for 5 h. The reaction mixture was neutralized with 1 M HCl and extracted into EtOAc (50 mL). The organic layer was washed with 10% aqueous NH_4Cl (50 mL), 10% aqueous $NaHCO_3$ (50 mL), and brine (50 mL). The organic layer was dried over $MgSO_4$, filtered, and concentrated under vacuum. The crude material was purified by column chromatography on silica gel (5–40% EtOAc/hexanes) to provide the title compound (mixture of diastereomers) as a light-brown viscous oil (132 mg, 87%). R_f = 0.15 (20% EtOAc/hexanes). HRMS (ESI, *m/z*): calcd for $[C_{22}H_{13}F_2O_2S]^+$ $(M-OH)^+$, 363.0650; found, 363.0649. An analytical sample was further separated to characterize each diastereomer individually.

Diastereomer 1:

^{1}H NMR (400 MHz, $CDCl_3$) δ: 2.85 (d, J_{HF} = 0.6 Hz, 2H, C_{11}), 3.29 (d, J_{HF} = 3.3 Hz, 2H, OH), 7.00 (s, 2H, C_9), 7.05 (ddd, J_{HF} = 11.6 Hz, J_{HH} = 8.1, 1.4 Hz, 2H, C_2), 7.16 (ddd, J_{HH} = 7.6, 7.6, 1.2 Hz, 2H, C_4), 7.33 (dddd, J_{HF} = 5.0 Hz, J_{HH} = 8.1, 7.5, 1.9 Hz, 2H, C_3), 7.67 (ddd, J_{HF} = 8.0 Hz, J_{HH} = 8.0, 1.7 Hz, 2H, C_5).

$^{13}C\{^{1}H\}$ NMR (101 MHz, $CDCl_3$) δ: 69.22 (C_7), 74.8 (d, J_{CF} = 2.4 Hz, C_{11}), 83.99 (C_{10}), 116.52 (d, J_{CF} = 21.7 Hz, C_2), 124.1 (d, J_{CF} = 3.6 Hz, C_4), 125.31 (d, J_{CF} = 1.5 Hz, C_9), 127.2 (d, J_{CF} = 2.2 Hz, C_5), 130.50 (d, J_{CF} = 10.0 Hz, C_6), 130.55 (d, J_{CF} = 8.5 Hz, C_3), 148.50 (C_8), 160.09 (d, J_{CF} = 249.4 Hz, C_1).

Diastereomer 2:

^{1}H NMR (400 MHz, $CDCl_3$) δ: 2.84 (d, J_{HF} = 0.6 Hz, 2H, C_{11}), 3.28 (d, J_{HF} = 3.0 Hz, 2H, OH), 6.94 (s, 2H, C_9), 7.05 (ddd, J_{HF} = 11.5 Hz, J_{HH} = 8.1, 1.4 Hz, 2H, C_2), 7.16 (ddd, J_{HH} = 7.6, 7.6, 1.2 Hz, 2H, C_4), 7.34 (dddd, J_{HF} = 5.0 Hz, J_{HH} = 8.1, 7.5, 1.8 Hz, 2H, C_3), 7.69 (ddd, J_{HF} = 8.0 Hz, J_{HH} = 8.0, 1.8 Hz, 2H, C_5).

$^{13}C\{^{1}H\}$ NMR (101 MHz, $CDCl_3$) δ: 69.18 (C_7), 74.9 (d, J_{CF} = 2.2 Hz, C_{11}), 84.03 (C_{10}), 116.51 (d, J_{CF} = 21.6 Hz, C_2), 124.1 (d, J_{CF} = 3.6 Hz, C_4), 125.27 (d, J_{CF} = 1.4 Hz, C_9), 127.3 (d, J_{CF} = 2.3 Hz, C_5), 130.4 (d, J_{CF} = 9.9 Hz, C_6), 130.57 (d, J_{CF} = 8.4 Hz, C_3), 148.47 (C_8), 160.06 (d, J_{CF} = 249.4 Hz, C_1).

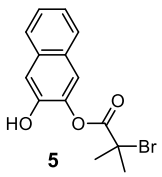

5

3-Hydroxynaphthalen-2-yl 2-bromo-2-methylpropanoate (5). An oven-dried round bottom flask equipped with a stir bar was charged with 2,3-dihydroxynaphthalene (3.0 g, 19 mmol) and evacuated/backfilled with nitrogen (3x). Anhydrous THF (54 mL) was added via syringe under nitrogen. The solution was cooled to 0 °C in an ice bath, followed by the consecutive dropwise addition of triethylamine (2.6 mL, 19 mmol) and α-bromoisobutyryl bromide (2.3 mL, 19 mmol) via syringe, resulting in formation of a white precipitate. The reaction mixture was allowed to warm to room temperature and stirred for 19 h. The mixture was extracted into EtOAc (120 mL) and washed with distilled water (50 mL) and brine (50 mL). The organic layer was dried over $MgSO_4$, filtered, and concentrated under reduced pressure. The crude material was purified by column chromatography on silica gel (5–38% EtOAc/hexanes) followed by recrystallization from EtOAc/hexanes to provide the title compound as colorless, transparent crystals (2.1 g, 36%).

TLC (20% EtOAc/hexanes): R_f = 0.38

^{1}H NMR (400 MHz, CD_2Cl_2) δ: 2.14 (s, 6H), 5.75 (s, 1H), 7.34 (d, *J* = 0.7 Hz, 1H), 7.38 (ddd, *J* = 8.1, 6.9, 1.3 Hz, 1H), 7.45 (ddd, *J* = 8.3, 6.9, 1.4 Hz, 1H), 7.62 (d, *J* = 0.7 Hz, 1H), 7.70 (ddddd, *J* = 8.2, 1.3, 0.6, 0.6, 0.6 Hz, 1H), 7.76 (ddddd, *J* = 8.2, 1.3, 0.7, 0.7, 0.7 Hz, 1H).

^{13}C{^{1}H} NMR (101 MHz, $CDCl_3$) δ: 30.8, 56.0, 112.3, 120.1, 124.5, 126.55, 126.58, 127.6, 128.6, 132.9, 138.7, 146.2, 170.0.

HRMS (ESI, *m/z*): calcd for $[C_{14}H_{17}{}^{79}BrO_3N]^+$ $(M-OH)^+$, 326.0386; found, 326.0388.

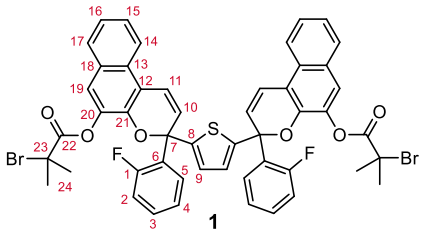

1

Thiophene-2,5-diylbis(3-(2-fluorophenyl)-3*H*-benzo[*f*]chromene-3,5-diyl) bis(2-bromo-2-methylpropanoate) (1). Naphthopyrans were synthesized according to the procedure by Zhao and Carreira.[1] A flame-dried two-neck round bottom flask equipped with a stir bar and condenser was charged with compound **5** (584 mg, 1.89 mmol) and pyridinium *p*-toluenesulfonate (20 mg, 0.080 mmol) and evacuated/ backfilled with nitrogen (3x). Compound **4** (290 mg, 0.762 mmol) dissolved in anhydrous 1,2-dichloroethane (5 mL) was added via syringe. Trimethyl orthoformate (0.38 mL, 3.5 mmol) was added via syringe and the solution was refluxed for 22 h. The solution was poured into water (50 mL) and extracted into EtOAc (50 mL). The organic layer was washed with 10% aqueous $NaHCO_3$ (50 mL), 10% aqueous NH_4Cl (50 mL), and brine (50 mL), dried over Na_2SO_4, filtered, and concentrated under reduced pressure. The crude product was purified by column chromatography (5–40% EtOAc/hexanes). It was further purified by precipitation from hexanes and isolated by filtration to provide the title compound (mixture of diastereomers) as a magenta powder (440 mg, 60%). R_f = 0.51 (20% EtOAC/hexanes). An analytical sample was separated by preparative HPLC to characterize each diastereomer individually.

Diastereomer 1:

^{1}H NMR (400 MHz, CD_2Cl_2) δ: 1.87 (s, 6H, C_{24}), 1.96 (s, 6H, C_{24}), 6.43 (dd, J_{HF} = 4.0 Hz, J_{HH} = 10.0 Hz, 2H, C_{10}), 6.90 (s, 2H, C_9), 7.02 (ddd, J_{HF} = 11.6 Hz, J_{HH} = 8.2, 1.2 Hz, 2H, C_2), 7.13 (ddd, J_{HF} = 7.4 Hz, J_{HH} = 7.9, 1.2 Hz, 2H, C_4), 7.25–7.35 (m, 4H, C_3 and C_{11}), 7.41 (ddd, J_{HH} = 8.0, 6.9, 1.2 Hz, 2H, C_{16}), 7.47–7.54 (m, 4H, C_{15} and C_{19}), 7.67 (ddd, J_{HF} = 8.0 Hz, J_{HH} = 8.0, 1.8 Hz, 2H, C_5), 7.72–7.76 (m, 2H, C_{17}), 7.97 (dd, J_{HH} = 8.7, 1.0 Hz, 2H, C_{14}).

^{13}C{^{1}H} NMR (101 MHz, CD_2Cl_2) δ: 31.3 (C_{24}), 31.4 (C_{24}), 55.6 (C_{23}), 79.2 (d, J_{CF} = 2.9 Hz, C_7), 115.9 (C_{12}), 117.00 (d, J_{CF} = 21.8 Hz, C_2), 120.3 (C_{11}), 121.17 (C_{19}), 121.97 (C_{14}), 124.45 (d, J_{CF} = 3.1 Hz, C_4), 125.4 (C_{16}), 126.1 (d, J_{CF} = 4.3 Hz, C_{10}), 126.3 (d, J_{CF} = 1.4 Hz, C_9), 127.3 (C_{15}), 127.6 (d, J_{CF} = 2.6 Hz, C_5), 128.4 (C_{18}), 128.71 (C_{17}), 129.4 (C_{12}), 130.69 (d, J_{CF} = 8.5 Hz, C_3), 131.0 (d, J_{CF} = 10.6 Hz, C_6), 139.39 (C_{20}), 142.5 (C_{21}), 148.5 (C_8), 159.6 (d, J_{CF} = 248.3 Hz, C_1), 170.3 (C_{22}).

HRMS (ESI, *m/z*): calcd for $[C_{50}H_{40}{}^{79}Br_2F_2O_6SN]^+$ $(M+NH_4)^+$, 978.0906; found, 978.0866.

Diastereomer 2:

^{1}H NMR (400 MHz, CD_2Cl_2) δ: 1.91 (s, 6H, C_{24}), 2.02 (s, 6H, C_{24}), 6.40 (dd, J_{HF} = 4.1 Hz, J_{HH} = 10.0 Hz, 2H, C_{10}), 6.78 (s, 2H, C_9), 7.01 (ddd, J_{HF} = 12.6 Hz, J_{HH} = 8.2, 1.1 Hz, 2H, C_2), 7.12 (ddd, J_{HF} = 7.4 Hz, J_{HH} = 7.9, 1.2 Hz, 2H, C_4), 7.27–7.34 (m, 4H, C_3 and C_{11}), 7.40 (ddd, J_{HH} = 8.1, 7.0, 1.1 Hz, 2H, C_{16}), 7.48–7.54 (m, 4H, C_{15} and C_{19}), 7.66 (ddd, J_{HF} = 8.0 Hz, J_{HH} = 8.0, 1.8 Hz, 2H, C_5), 7.68–7.72 (m, 2H, C_{17}), 7.96 (dd, J_{HH} = 8.7, 1.0 Hz, 2H, C_{14}).

^{13}C{^{1}H} NMR (101 MHz, CD_2Cl_2) δ: 31.3 (C_{24}), 31.4 (C_{24}), 55.7 (C_{23}), 79.6 (d, J_{CF} = 2.6 Hz, C_7), 116.1 (C_{12}), 117.02 (d, J_{CF} = 22.0 Hz, C_2), 120.1 (C_{11}), 121.22 (C_{19}), 121.99 (C_{14}), 124.41 (d, J_{CF} = 3.2 Hz, C_4), 125.4 (C_{16}), 125.7 (d, J_{CF} = 1.7 Hz, C_9), 126.7 (d, J_{CF} = 4.0 Hz, C_{10}), 127.3 (C_{15}), 128.0 (d, J_{CF} = 2.8 Hz, C_5), 128.4 (C_{18}), 128.69 (C_{17}), 129.4 (C_{12}), 130.66 (d, J_{CF} = 10.7 Hz, C_6), 130.8 (d, J_{CF} = 8.4 Hz, C_3), 139.44 (C_{20}), 142.6 (C_{21}), 148.7 (C_8), 159.9 (d, J_{CF} = 248.7 Hz, C_1), 170.4 (C_{22}).

HRMS (ESI, *m/z*): calcd for $[C_{50}H_{40}{}^{79}Br_2F_2O_6SN]^+$ $(M+NH_4)^+$, 978.0906; found, 978.0861.

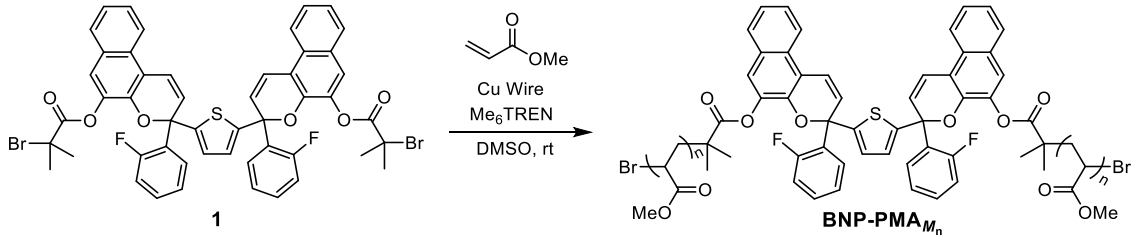

General Procedure for the Synthesis of Polymers Incorporating a Bis-Naphthopyran Mechanophore

A representative procedure is provided for the synthesis of **BNP-PMA$_{73}$**. A 10 mL flame-dried Schlenk flask equipped with a stir bar was charged with initiator **1** (18.3 mg, 0.0204 mmol), DMSO (1.00 mL), methyl

acrylate (2.00 mL, 22.2 mmol) and freshly cut copper wire (2.0 cm, 20 gauge). The flask was sealed, the solution was degassed via four freeze-pump-thaw cycles, and then backfilled with nitrogen and warmed to room temperature. Me_6TREN (10.5 µL, 0.0393 mmol) was added via microsyringe. After stirring at room temperature for 2 h, the flask was opened to air and the solution was diluted with DCM. The polymer solution was precipitated into methanol cooled with dry ice (3x) and the isolated material was dried under vacuum to provide 1.05 g of polymer (55%). M_n = 73.2 kg/mol, $Đ$ = 1.10.

Scheme S2. Synthesis of chain-end functional control polymer **BNP-PMA$_{Control}$**.

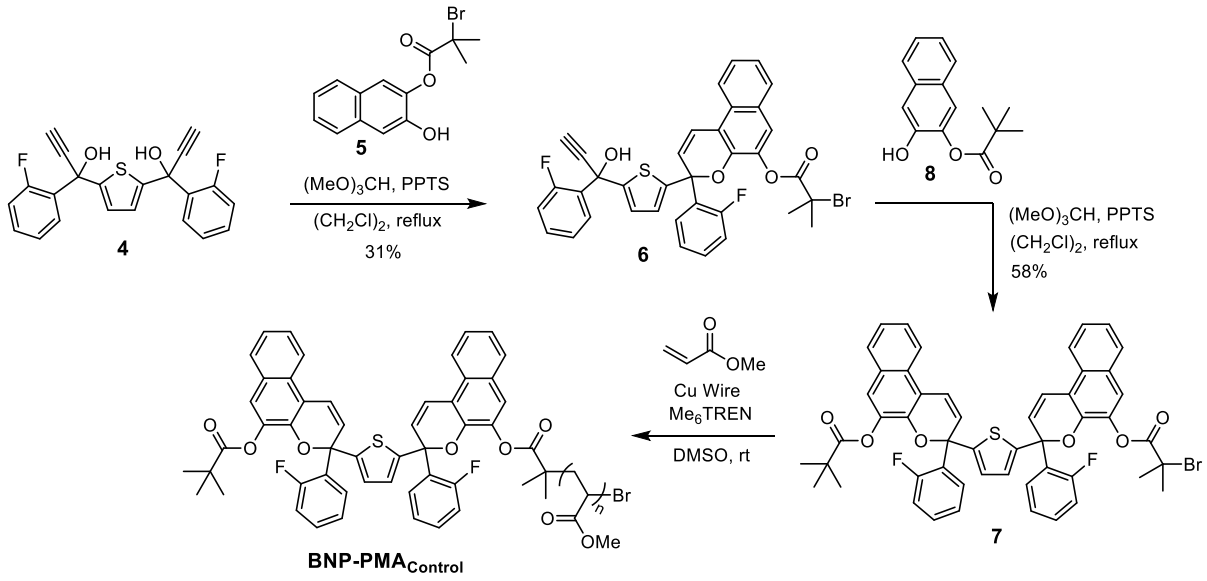

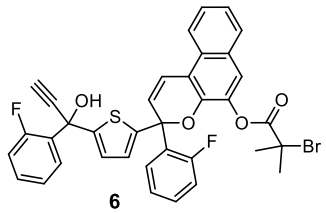

3-(2-fluorophenyl)-3-(5-(1-(2-fluorophenyl)-1-hydroxyprop-2-yn-1-yl)thiophen-2-yl)-3*H*-benzo[*f*]chromen-5-yl 2-bromo-2-methylpropanoate (6). A flame-dried two-neck round bottom flask equipped with a condenser and stir bar was charged with compound **5** (594 mg, 1.92 mmol) and pyridinium *p*-toluenesulfonate (27 mg, 0.11 mmol) and evacuated/ backfilled with nitrogen (3x). Compound **4** (729 mg, 1.92 mmol) was dissolved in 1,2-dichloroethane (20 mL) under nitrogen and added to the reaction mixture, followed by addition of trimethyl orthoformate (0.95 mL, 2.7 mmol) via syringe. The reaction was refluxed for 14 h, during which time it became a deep red color. The solution was cooled to room temperature, concentrated under reduced pressure, and dissolved in EtOAc (50 mL). The organic layer was washed with distilled water (50 mL), 1 M aqueous $NaHCO_3$ (50 mL), and brine (50 mL). The organic layer was dried over $MgSO_4$, filtered, and concentrated under reduced pressure. The crude product was purified by column chromatography on silica gel (20–100% DCM/hexanes) to provide the title compound (mixture of diastereomers) as a red foamy solid (400 mg, 31%).

TLC (100% DCM): R_f = 0.32

^{1}H NMR (400 MHz, CD_2Cl_2) δ: 2.00 (s, 1.5H), 2.03 (s, 1.5H), 2.08 (s, 1.5H), 2.10 (s, 1.5H), 2.85 (d, J_{HF} = 0.8 Hz, 0.5H), 2.86 (d, J_{HF} = 0.7 Hz, 0.5H), 3.33 (d, J_{HF} = 1.2 Hz, 0.5H), 3.34 (d, J_{HF} = 1.4 Hz, 0.5H), 6.47 (dd, J_{HF} = 3.9 Hz, J_{HH} = 10.0, 1H), 6.47 (dd, J_{HF} = 3.9 Hz, J_{HH} = 10.0, 1H), 6.85 (d, J_{HH} = 3.8 Hz, 0.5H), 6.90 (d, J_{HH} = 3.8 Hz, 0.5H), 6.92–6.97 (m, 1H), 6.99–7.09 (m, 2H), 7.11–7.21 (m, 2H), 7.29–7.38 (m, 3H), 7.38–7.45 (m, 1H), 7.48–7.56 (m, 2H), 7.63 (dddd, , J_{HF} = 8.0 Hz, J_{HH} = 9.6, 7.8, 1.8 Hz, 1H), 7.70–7.79 (m, 2H), 7.96–8.03 (m, 1H).

^{13}C{^{1}H} NMR (151 MHz, CD_2Cl_2) δ: 31.41, 31.42, 31.45, 55.7 (d, J_{CF} = 2.9 Hz), 69.2, 69.3, 74.8 (d, J_{CF} = 2.5 Hz), 74.9 (d, J_{CF} = 2.4 Hz), 79.3 (d, J = 2.7 Hz), 79.4 (d, J_{CF} = 2.9 Hz), 84.5, 116.20, 116.21, 116.79 (d, J_{CF} = 21.8 Hz), 116.79 (d, J_{CF} = 21.8 Hz), 117.05 (d, J_{CF} = 21.9 Hz), 117.07 (d, J_{CF} = 21.8 Hz), 120.46, 120.53, 121.30, 121.32, 122.0, 124.5 (d, J_{CF} = 3.1 Hz), 124.6 (d, J_{CF} = 4.7 Hz), 125.5, 125.66 (d, J_{CF} = 1.0 Hz), 125.70 (d, J_{CF} = 0.8 Hz), 126.0 (d, J_{CF} = 1.3 Hz), 126.1 (d, J_{CF} = 1.2 Hz), 126.2 (d, J_{CF} = 4.2 Hz), 126.4 (d, J_{CF} = 4.5 Hz), 127.4, 127.5 (d, J_{CF} = 2.3 Hz), 127.6 (d, J_{CF} = 2.3 Hz), 127.7 (d, J_{CF} = 2.6 Hz), 127.9 (d, J_{CF} = 2.8 Hz), 128.5, 128.7, 129.4, 130.77 (d, J_{CF} = 10.6 Hz), 130.79 (d, J_{CF} = 8.4 Hz), 130.81 (d, J_{CF} = 8.4 Hz), 130.9 (d, J_{CF} = 10.6 Hz), 130.97 (d, J_{CF} = 8.4 Hz), 131.00 (d, J_{CF} = 8.5 Hz), 131.10 (d, J_{CF} = 10.2 Hz), 131.13 (d, J_{CF} = 10.1 Hz), 139.5, 142.58, 142.59, 148.1, 148.3, 149.47, 149.51, 159.79 (d, J_{CF} = 248.1 Hz), 159.84 (d, J_{CF} = 248.4 Hz), 160.40 (d, J_{CF} = 249.3 Hz), 160.44 (d, J_{CF} = 249.4 Hz), 170.53.

HRMS (ESI, *m/z*): calcd for $[C_{36}H_{29}{}^{79}BrF_2O_4SN]^+$ $(M+NH_4)^+$, 688.0963; found, 688.0946.

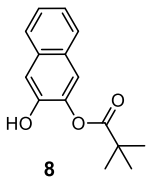

8

3-hydroxynaphthalen-2-yl pivalate (8). A flame-dried two neck round bottom flask equipped with a stir bar was charged with 2,3-dihydroxynaphthalene (3.00 g, 18.7 mmol) and evacuated/backfilled with nitrogen (3x). Anhydrous THF (30 mL) was added via syringe under nitrogen. The solution was cooled to 0 °C in an ice bath, followed by the consecutive dropwise addition of triethylamine (2.65 mL, 19.0 mmol) and pivaloyl chloride (2.30 mL, 18.7 mmol) via syringe, resulting in formation of a white precipitate. The reaction mixture was allowed to warm to room temperature and stirred for 16 h. The precipitate was filtered off and rinsed with EtOAc (100 mL), and the filtrate was collected and washed with DI water (50 mL), 10% aqueous NH_4Cl (50 mL), and brine (50 mL). The organic layer was dried over Na_2SO_4, filtered, and concentrated under reduced pressure. The crude product was purified by column chromatography on silica gel (DCM) to provide the title compound as white crystals (3.10 g, 68%).

TLC (100% DCM): R_f = 0.84

^{1}H NMR (400 MHz, CD_2Cl_2) δ: 1.43 (s, 9H), 7.32 (s, 1H), 5.36–5.39 (m, 1H), 7.36 (ddd, J = 8.1, 6.9, 1.3 Hz, 1H), 7.42 (ddd, J = 8.2, 6.9, 1.4 Hz, 1H), 7.55 (d, J = 0.7, 1H), 7.69 (app br d, J = 8.1 Hz, 1H), 7.74 (ddddd, J = 8.1, 1.3, 0.6, 0.6, 0.6 Hz, 1H).

$^{13}C\{^{1}H\}$ NMR (101 MHz, $CDCl_3$) δ: 27.4, 39.6, 112.5, 120.0, 124.4, 126.2, 126.4, 127.4, 128.8, 132.6, 139.8, 146.3, 177.4.

HRMS (ESI, *m/z*): calcd for $[C_{15}H_{20}O_3N]^+$ $(M+NH_4)^+$, 262.1438; found, 262.1439.

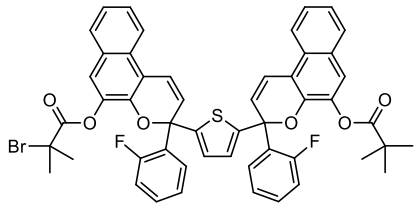

7

3-(5-(5-((2-bromo-2-methylpropanoyl)oxy)-3-(2-fluorophenyl)-3*H*-benzo[*f*]chromen-3-yl)thiophen-2-yl)-3-(2-fluorophenyl)-3*H*-benzo[*f*]chromen-5-yl pivalate (7). A flame-dried two-neck round bottom flask equipped with a condenser and stir bar was charged with compound **8** (51 mg, 0.21 mmol) and pyridinium *p*-toluenesulfonate (2.7 mg, 0.011 mmol) and evacuated/backfilled with nitrogen (3x). Compound **6** (71 mg, 0.11 mmol) was dissolved in anhydrous 1,2-dichloroethane (2.5 mL) under nitrogen and added to the reaction mixture, followed by addition of trimethyl orthoformate (50 µL, 0.46 mmol) via syringe. The reaction was refluxed for 12 h. The solution was cooled to room temperature, extracted into EtOAc (20 mL), and washed with 10% aqueous NH_4Cl (20 mL), 1 M aqueous $NaHCO_3$ (20 mL), and brine (20 mL). The organic layer was dried over Na_2SO_4, filtered, and concentrated under reduced pressure. The crude product was purified by consecutive chromatographic separations on silica gel (10–40% EtOAc/hexanes, then 40–80% DCM/hexanes) to provide the title compound (mixture of diastereomers) as a red foamy solid (55 mg, 58%).

TLC (20% EtOAc/hexanes): R_f = 0.47

^{1}H NMR (400 MHz, CD_2Cl_2) δ: 1.25 (s, 4.5H)**,** 1.30 (s, 4.5H), 1.87 (s, 1.5H), 1.93 (s, 1.5H), 1.97 (s, 1.5H), 2.03 (s, 1.5H), 6.38–6.47 (m, 2H), 6.76–6.81 (m, 1H), 6.90 (s, 1H), 6.98–7.06 (m, 2H), 7.09–7.17 (m, 2H), 7.25–7.35 (m, 4H), 7.36–7.56 (m, 6H), 7.63–7.76 (m, 4H), 7.91–7.99 (m, 2H).

$^{13}C\{^{1}H\}$ NMR (101 MHz, CD_2Cl_2) δ: 27.6, 31.31, 31.32, 31.35, 39.41, 39.5, 55.7, 55.8, 79.0 (d, J = 3.0 Hz), 79.2 (d, J_{CF} = 2.9 Hz), 79.4 (d, J_{CF} = 2.8 Hz), 79.6 (d, J_{CF} = 2.6 Hz), 115.6, 115.8, 115.9, 116.1, 116.97 (d, J_{CF} = 21.8 Hz), 116.98 (d, J_{CF} = 21.8 Hz), 117.02 (d, J_{CF} = 21.9 Hz), 120.12, 120.14, 120.3, 120.4, 121.16, 121.21, 121.5, 121.6, 121.91, 121.93, 121.98, 122.00, 124.39 (d, J_{CF} = 3.0 Hz), 124.42 (d, J_{CF} = 2.8 Hz), 125.2, 125.4, 125.7 (d, J = 1.6 Hz), 125.8 (d, J_{CF} = 1.7 Hz), 125.9 (d, J_{CF} = 4.5 Hz), 126.1 (d, J_{CF} = 4.4 Hz), 126.2 (d, J_{CF} = 1.3 Hz), 126.3 (d, J_{CF} = 1.4 Hz), 126.5 (d, J_{CF} = 4.2 Hz), 126.7 (d, J_{CF} = 3.9 Hz), 127.0, 127.3, 127.58 (d, J_{CF} = 2.5 Hz), 127.59 (d, J_{CF} = 2.9 Hz), 127.9 (d, J_{CF} = 3.0 Hz), 128.0 (d, J_{CF} = 2.7 Hz), 128.2, 128.4, 128.5, 128.6, 128.69, 128.70, 129.4, 129.5, 130.6 (d, J_{CF} = 8.5 Hz), 130.7 (d, J_{CF} = 8.1 Hz), 130.8 (d, J_{CF} = 8.6 Hz), 130.9 (d, J_{CF} = 10.8 Hz), 131.1 (d, J_{CF} = 10.7 Hz), 131.2 (d, J_{CF} = 10.9 Hz), 139.4, 139.5, 139.96, 140.01, 142.55, 142.61, 142.9, 143.0, 148.5, 148.69, 148.71, 148.8, 159.6 (d, J_{CF} = 248.2 Hz), 159.7 (d, J_{CF} = 248.3 Hz), 159.8 (d, J_{CF} = 248.5 Hz), 159.9 (d, J_{CF} = 248.7 Hz), 170.35, 170.41, 176.90, 176.92.

HRMS (ESI, *m/z*): calcd for $[C_{51}H_{43}{}^{79}Br_2F_2O_6SN]^+$ $(M+NH_4)^+$, 914.1957; found, 914.1921.

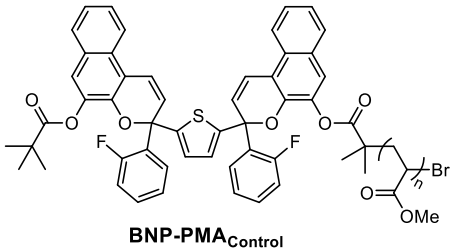

BNP-PMA$_{Control}$

Chain-end control polymer (BNP-PMA$_{Control}$). A PMA control polymer containing the bis-naphthopyran mechanophore at the chain-end was synthesized following the general procedure using initiator **7** (19.9 mg, 0.0222 mmol), DMSO (1.20 mL), methyl acrylate (2.40 mL, 26.7 mmol) and freshly cut copper wire (2.0 cm, 20 gauge) to provide 1.18 g of polymer (51%). M_n = 71.2 kg/mol, $Đ$ = 1.14.

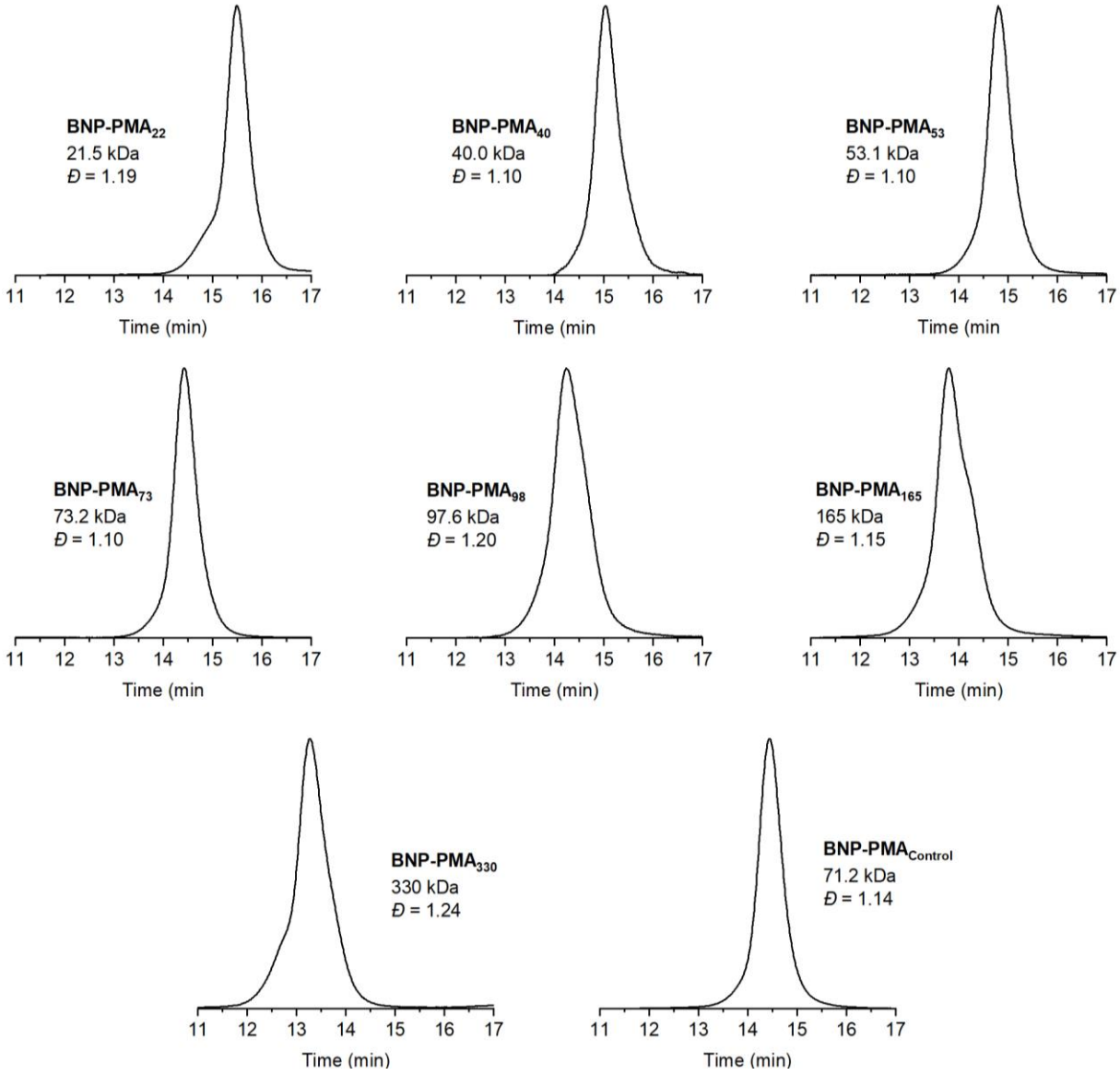

Figure S5. GPC traces (refractive index response), M_n, and dispersity for each polymer studied.

IV. DFT Calculations (CoGEF)

CoGEF calculations were performed using Spartan ′18 Parallel Suite according to previously reported methods.[2-4] Ground state energies were calculated using DFT at the B3LYP/6-31G* level of theory. For both possible diastereomers, the equilibrium conformations of the unconstrained molecules were initially calculated followed by optimization of the equilibrium geometries. Starting from the equilibrium geometry of the unconstrained molecules (energy = 0 kJ/mol), the distance between the terminal methyl groups of the truncated structures was increased in increments of 0.05 Å and the energy was minimized at each step (Figure S6). The maximum force associated with the electrocylic ring-opening reactions was calculated from the slope of the curve immediately prior to C–O bond cleavage. For the S,S-diastereomer, the first ring-opening event is predicted to occur at a maximum force of 4.1 nN and the

second occurs at 4.6 nN. For the R,S-diastereomer, the respective forces are 4.1 nN and 4.5 nN for the first and second ring-opening reactions. The relatively small energetic relaxations observed between the two ring-opening transformations correspond to conformational rotations around a single bond in the merocyanine structures.

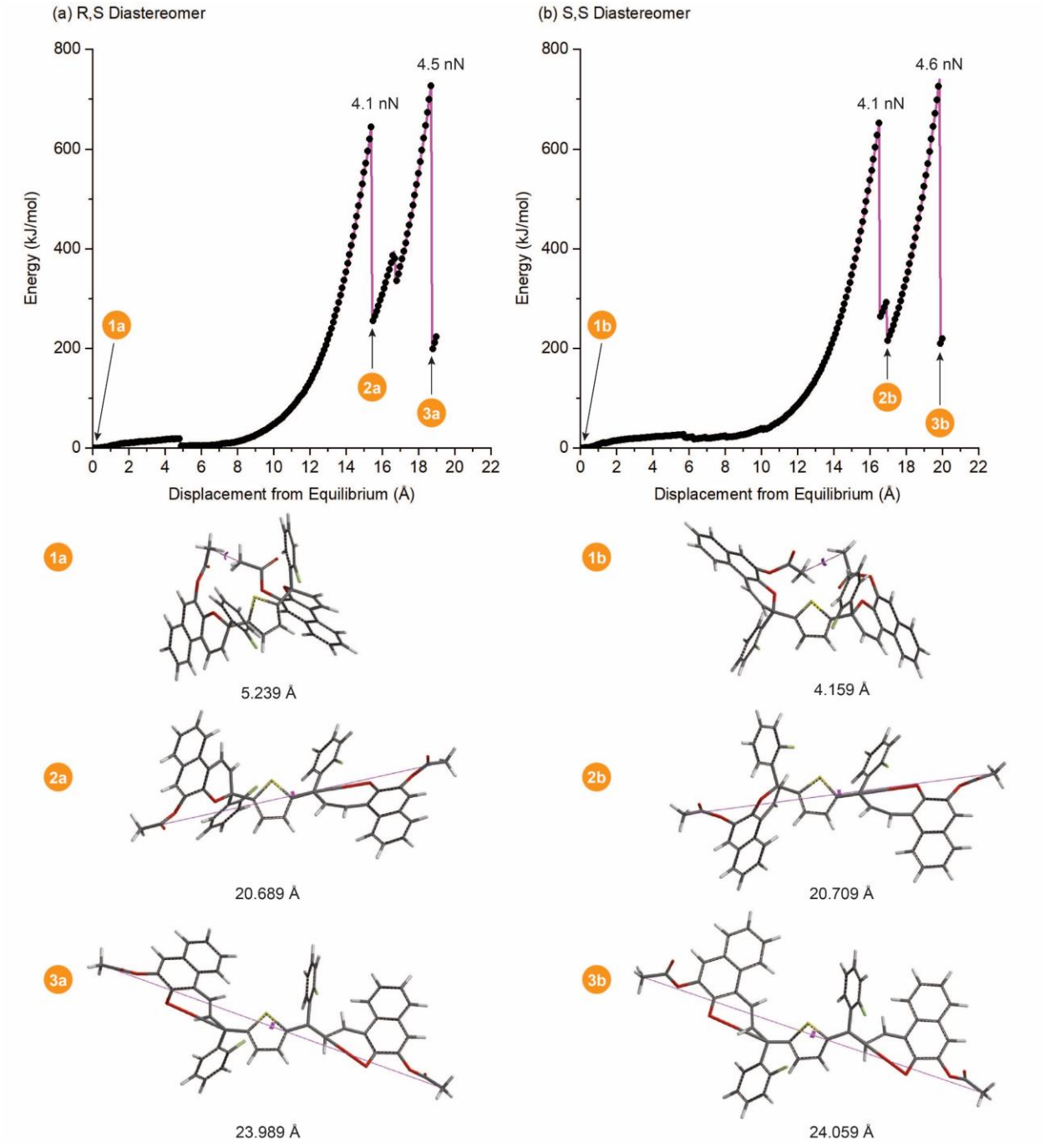

Figure S6. DFT calculations using the constrained geometries simulate external force (CoGEF) method at the B3LYP/6-31G* level of theory for the (a) R,S-diastereomer and (b) S,S-diastereomer of the bis-naphthopyran mechanophore. The corresponding computed structures of the truncated molecules at various points of elongation are shown along with the associated constraint distance between the terminal methyl groups.

V. Details for Photoirradiation and Sonication Experiments

In order to continuously monitor reaction progress by UV-vis absorption spectroscopy, an experimental setup based on previously reported design[5] was assembled using a peristaltic pump to transport solution from the reaction vessel through a quartz flow cell in a UV-vis spectrometer and return the solution to the reaction vessel. The flow rate through the system was maintained at 6 mL/min, corresponding to a setting of 50 RPM on the peristaltic pump. The UV-vis spectrometer was programmed to acquire either full spectra or absorbance at predefined wavelengths at regular time intervals. Absorbance measurements at wavelengths of 460 nm, 620 nm, and 800 nm were acquired every ten seconds during continuous photoirradiation or sonication of polymer solutions. The absorbance values measured at 800 nm were subtracted from the absorbance values monitored at 460 nm and 620 nm at each time point to account for drift during the experiments. Absorbance data was baseline corrected by subtracting the initial absorbance value (t = 0) at each wavelength; however, this step was omitted for determining the concentrations of merocyanine species.

General procedure for photoirradiation experiments. An oven-dried sonication vessel was fitted with a Teflon screw cap sealed with an O-ring and allowed to cool under a stream of dry argon. The vessel was charged with a solution of the polymer in THF (2.0 mg/mL, 20.0 mL). An additional 6.2 mL of polymer solution was pumped into the dead space of the circulatory setup. Teflon inlet and outlet tubes were inserted into the solution in the reaction vessel through a plastic cap sealed with parafilm, and the pump was engaged to start the flow of solution through the system. The sonication vessel was submerged in an ethanol bath maintained at −45 ± 2 °C and a UV light source (λ = 311 nm) was placed 2 inches from the vessel. The total volume of the apparatus was 26.2 mL, with 20.0 mL contained in the reaction vessel. At any given time, only 20.0 mL of solution (out of the total 26.2 mL) was inside of the cuvette and exposed to UV irradiation. Therefore, the actual "irradiation time" was treated as 20/26.2 of real "clock" time, consistent with previously reported methods.[5] The entire system was protected from outside light for the duration of the experiment.

General procedure for sonication experiments. An oven-dried sonication vessel was placed onto the sonication probe and allowed to cool under a stream of dry argon. The vessel was charged with a solution of the polymer in THF (2.0 mg/mL, 20.0 mL). An additional 6.2 mL of polymer solution was pumped into the dead space of the circulatory setup. Teflon inlet and outlet tubes were inserted into the solution in the sonication vessel through a plastic cap sealed with parafilm, and the pump was engaged to start the flow of solution through the system. The sonication vessel was submerged in an acetone bath maintained at −45 ± 2 °C. The polymer solution was sparged with argon for 30 minutes prior to sonication and for the duration of the sonication experiment. Solutions were sonicated continuously at 20 kHz (8.20 W cm^{-2}). Sonication intensity was calibrated via the literature method.[6] Similar to the photoirradiation experiments described above, "sonication time" was treated as 20/26.2 of real "clock" time to account for the fraction of polymer solution actually exposed to ultrasound during the experiment. The entire system was kept in the dark for the duration of the experiment.

VI. Description of Control Experiments

To confirm that the ring-opening reactions observed for chain-centered BNP molecules exposed to ultrasonication were due to mechanical force,[7] a chain-end functional control polymer (**BNP-PMA$_{Control}$**) was synthesized and sonicated under identical conditions. As shown in Figure S2, no changes in absorption were detected during sonication of the chain-end functional control polymer.

All sonication experiments were performed using polymer solutions with a concentration of 2 mg/mL. A set of control experiments were performed to confirm that changes in the molar concentration of polymers as a result of varying molecular weight at constant mass concentration were not responsible for observed variation in the ratio B_{620}/B_{460} (Figure S7). Solutions of **BNP-PMA$_{73}$** were prepared at 1 mg/mL and 3 mg/mL in THF and sonicated under the same conditions as the 2 mg/mL solution. The average ratios of B_{620}/B_{460} from two separate trials were determined to be 0.44 and 0.43 for concentrations of 1 mg/mL, and 3 mg/mL, respectively, compared to the value of 0.44 measured for the 2 mg/mL solution. These data indicate that variation in the molar concentration of polymers in this range does not significantly affect the distribution of merocyanine products.

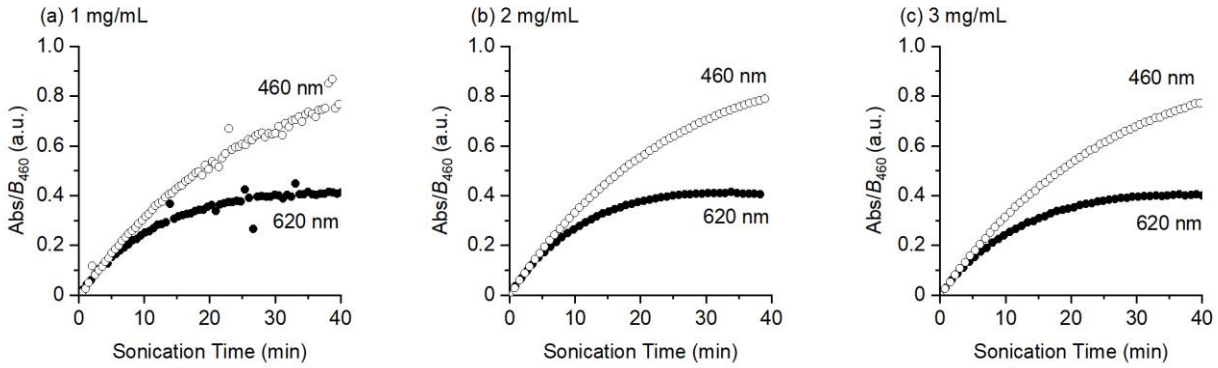

Figure S7. Absorbance at 460 nm and 620 nm measured as function of sonication time for **BNP-PMA$_{73}$** in THF at −45 °C at three different concentrations: (a) 1 mg/mL, (b) 2 mg/mL, (c) 3 mg/mL.

VII. Modeling Force-Dependent Absorption

We constructed a theoretical model to describe the force-color relationship observed for the BNP mechanophore. We use the ratio of the steady-state absorbance at 620 nm (B_{620}) to the steady-state absorbance at 460 nm (B_{460}) as a proxy for the overall distribution of the two distinct merocyanine products resulting from mechanochemical reaction. We first establish that this ratio, B_{620}/B_{460}, scales with the relative concentrations of $BNP_{O\text{-}O}$ and $BNP_{O\text{-}C}$, which are calculated from the experimentally determined absorbance values at 460 nm and 620 nm using the Beer-Lambert relationship and extinction coefficients estimated from similar isolated merocyanine molecules. Based on the reported spectra for isolated merocyanines derived from analogous thiophene-linked[8] and bithiophene-linked[9] bis-naphthopyrans, we estimate the following extinction coefficients, ε, for $BNP_{O\text{-}C}$ and $BNP_{O\text{-}O}$:

	Wavelength (nm)	ε (L mol^{-1} cm^{-1})
BNP$_{O\text{-}C}$	460	26,000
BNP$_{O\text{-}O}$	460	30,000
	620	23,000

The mathematical relationship between absorbance at 460 nm and 620 nm and the concentrations of $BNP_{O\text{-}C}$ and $BNP_{O\text{-}O}$ is given by eq S1:

$$\frac{Abs_{t,460}}{Abs_{t,620}} = \frac{\varepsilon_{O\text{–}C,460}[BNP_{O\text{–}C}]_t + \varepsilon_{O\text{–}O,460}[BNP_{O\text{–}O}]_t}{\varepsilon_{O\text{–}O,620}[BNP_{O\text{–}O}]_t} \quad \text{(S1)}$$

where $Abs_{t,460}$ is the absorbance value measured at 460 nm and time t, $\varepsilon_{O\text{–}C,460}$ is the extinction coefficient of $BNP_{O\text{-}C}$ at 460 nm, $[BNP_{O\text{–}C}]_t$ is the concentration of $BNP_{O\text{-}C}$ at time t, etc. The expression simplifies to the following linear function in slope-intercept form:

$$\frac{Abs_{t,460}}{Abs_{t,620}} = \frac{\varepsilon_{O\text{–}C,460}}{\varepsilon_{O\text{–}O,620}}\frac{[BNP_{O\text{–}C}]_t}{[BNP_{O\text{–}O}]_t} + R_{O\text{–}O} \quad \text{(S2)}$$

where $R_{O\text{-}O}$ is a constant defined by eq (S3):

$$R_{O\text{–}O} = \frac{\varepsilon_{O\text{–}O,460}}{\varepsilon_{O\text{–}O,620}} \quad \text{(S3)}$$

We define the relative steady-state concentrations of $BNP_{O\text{-}C}$ and $BNP_{O\text{-}O}$ by equations S4 and S5:

$$\varphi_{O\text{–}O} = \frac{[BNP_{O\text{–}O}]}{[BNP_{O\text{–}C}] + [BNP_{O\text{–}O}]} \quad \text{(S4)}$$

$$\varphi_{O\text{–}O} + \varphi_{O\text{–}C} = 1 \quad \text{(S5)}$$

Combining equations S2, S4, and S5 gives eq S6:

$$\frac{B_{460}}{B_{620}} = \frac{\varepsilon_{O\text{–}C,460}}{\varepsilon_{O\text{–}O,620}}\frac{(1-\varphi_{O-O})}{\varphi_{O-O}} + R_{O\text{–}O} \quad \text{(S6)}$$

where B_{460} and B_{620} are the steady-state absorbance values at 460 nm and 620 nm, respectively, determined from fitting the absorbance–time data to an increasing exponential decay function as described in the main text. The ratio of absorbance values at the mechanostationary state, which provides a description of the overall color of the system, is derived in terms of the relative concentration of $BNP_{O\text{-}O}$. Furthermore, as the concentration of $BNP_{O\text{-}O}$ becomes large (relative to $BNP_{O\text{-}C}$), the absorbance ratio B_{460}/B_{620} approaches a constant value, $R_{O\text{-}O}$.

We next derive a relationship to approximate the dependence of the relative concentration of $BNP_{O\text{-}O}$ on the degree of polymerization (DP), or M_n, of the attached polymer chains (DP = M_n/M_0). Mechanochemical reactions are described by first-order kinetics with respect to DP, whereby the rate of mechanochemical activation is directly proportional to DP above a threshold chain length.[3,5] The combined experimental and computational data indicate that the relative concentration of $BNP_{O\text{-}O}$

increases with longer polymer chains, and hence greater applied force.[10] Thus, the relative concentration of $BNP_{O\text{-}O}$ at the steady-state can be approximated by eq S7:

$$\varphi_{OO} = A(1 - e^{-c(M_n/M_0)}) \tag{S7}$$

where the constant c is a fit-determined parameter that modifies the dependence of the changing concentration on DP, and the pre-exponential factor, A, is equal to 100% from eq S5. The value of c was determined to be 9×10^{-4}.

Equations S6 and S7 are then combined to give eq S8, which expresses the dependence of the ratio B_{460}/B_{620} on DP:

$$\frac{B_{460}}{B_{620}} = \frac{\varepsilon_{\text{O–C},460}}{\varepsilon_{\text{O–O},620}} \frac{\left(e^{-c(\frac{M_n}{M_0})}\right)}{\left(1 - e^{-c(\frac{M_n}{M_0})}\right)} + R_{\text{O–O}} \tag{S8}$$

Up until this point we have derived the relationships relating the ratio B_{460}/B_{620} because it simplifies the expressions; however, it is more intuitive to discuss the increasing ratio of B_{620}/B_{460} as degree of polymerization increases. We therefore take the reciprocal of eq S8, which provides the relationship between the ratio of the steady-state absorption values and DP, or M_n, of the polymer according to eq S9:

$$\frac{B_{620}}{B_{460}} = \left(\frac{\varepsilon_{\text{O–C},460}}{\varepsilon_{\text{O–O},620}} \frac{\left(e^{-c(\frac{M_n}{M_0})}\right)}{\left(1 - e^{-c(\frac{M_n}{M_0})}\right)} + R_{\text{O–O}} \right)^{-1} \tag{S9}$$

The ratio B_{620}/B_{460} is predicted to increase asymptotically toward a value of $\frac{1}{R_{\text{O–O}}}$, or $\frac{\varepsilon_{\text{O–O},620}}{\varepsilon_{\text{O–O},460}}$, as DP becomes infinitely large.

VIII. Kinetic Modeling

Scheme S3. Proposed mechanism for the dynamic equilibrium achieved upon mechanochemical activation of the bis-naphthopyran mechanophore and associated rate constants for each step.

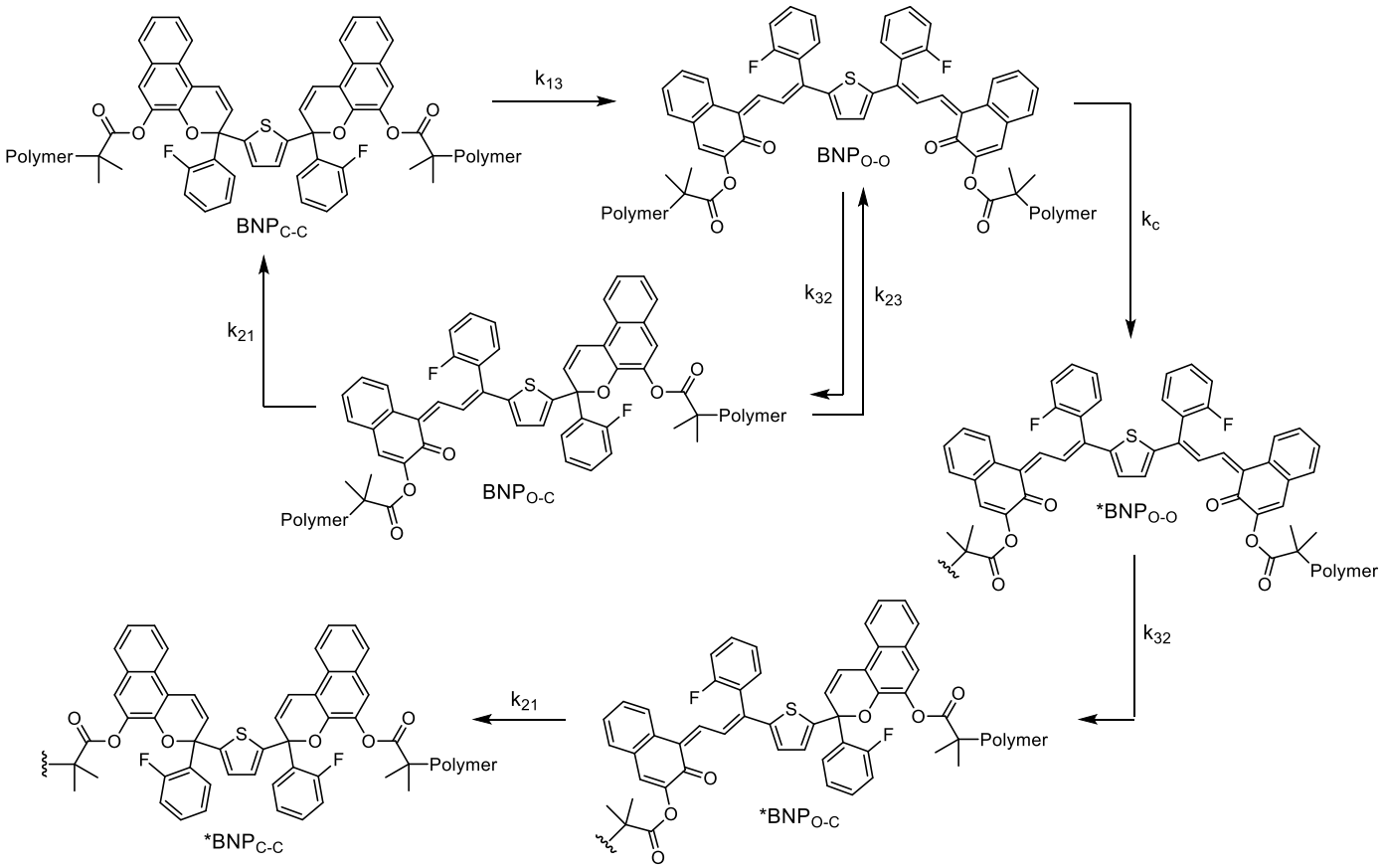

The mechanochemical reactivity of the bis-naphthopyran mechanophore in our system is consistent with the mechanism shown in Scheme S3. As detailed below, numerical modeling of the rate expressions describing this system of reactions supports this proposed mechanism in which BNP_{C-C} is effectively converted directly to BNP_{O-O}, in contrast to the photochemical reaction. Biased by external force, BNP_{C-C} exists in equilibrium with BNP_{O-C} and BNP_{O-O} and the distribution of the two merocyanine species is dictated by the balance between the forward rate of mechanochemical activation and thermal electrocyclization. The kinetic model suggests that BNP_{O-C} is produced predominately, if not exclusively, from thermal electrocyclization of BNP_{O-O}. The data and the kinetic model also indicate that BNP_{O-C} can be activated mechanochemically to regenerate BNP_{O-O}. Polymer chain scission occurs for most polymers with extended ultrasonication, leading to irreversible loss of BNP_{O-O}. The products resulting from chain cleavage (described by rate constant k_c) are denoted with an asterisk (e.g., $*BNP_{O-O}$). Polymers that undergo chain scission cannot be reactivated by ultrasonication, leading to an irreversible degradation pathway that results in loss of merocyanine via thermal electrocyclization. The corresponding rate expressions for the system of reactions shown in Scheme S3 are outlined below in equations S10–S15:

$$\frac{d[\mathrm{BNP_{C\text{-}C}}]_t}{dt} = -k_{13}[\mathrm{BNP_{C\text{-}C}}]_t + k_{21}[\mathrm{BNP_{O\text{-}C}}]_t \quad \text{(S10)}$$

$$\frac{d[\mathrm{BNP_{O\text{-}C}}]_t}{dt} = k_{32}[\mathrm{BNP_{O\text{-}O}}]_t - k_{23}[\mathrm{BNP_{O\text{-}C}}]_t - k_{21}[\mathrm{BNP_{O\text{-}C}}]_t \quad \text{(S11)}$$

$$\frac{d[\mathrm{BNP_{O\text{-}O}}]_t}{dt} = k_{13}[\mathrm{BNP_{C\text{-}C}}]_t + k_{23}[\mathrm{BNP_{O\text{-}C}}]_t - k_{32}[\mathrm{BNP_{O\text{-}O}}]_t - k_c[\mathrm{BNP_{O\text{-}O}}]_t \quad \text{(S12)}$$

$$\frac{d[{}^*\mathrm{BNP_{O\text{-}O}}]_t}{dt} = k_c[\mathrm{BNP_{O\text{-}O}}]_t - k_{32}[{}^*\mathrm{BNP_{O\text{-}O}}]_t \quad \text{(S13)}$$

$$\frac{d[{}^*\mathrm{BNP_{O\text{-}C}}]_t}{dt} = k_{32}[{}^*\mathrm{BNP_{O\text{-}O}}]_t - k_{21}[{}^*\mathrm{BNP_{O\text{-}C}}]_t \quad \text{(S14)}$$

$$\frac{d[{}^*\mathrm{BNP_{C\text{-}C}}]_t}{dt} = k_{21}[{}^*\mathrm{BNP_{O\text{-}C}}]_t \quad \text{(S15)}$$

The integrated rate law from the system of differential rate equations was solved numerically using the *ParametricNDSolve* function in Wolfram Mathematica 12[11] following the procedure by Collum.[12] The *ParametricNDSolve* function was chosen to allow rate constants to be free parameters. The results provided from the numerical solution of the integrated rate law allow for direct comparison of the expected changes in the concentration of merocyanine species to experimental data. In order to model time-dependent changes in absorbance, the relationships shown in equations S16 and S17 were employed to convert concentrations to absorbance values using the extinction coefficients presented previously in section VII.

$$Abs_{460} = \varepsilon_{\mathrm{O\text{-}C},460}[\mathrm{BNP_{O\text{-}C}}]_t + \varepsilon_{\mathrm{O\text{-}C},460}[{}^*\mathrm{BNP_{O\text{-}C}}]_t + \varepsilon_{\mathrm{O\text{-}O},460}[\mathrm{BNP_{O\text{-}O}}]_t + \varepsilon_{\mathrm{O\text{-}O},460}[{}^*\mathrm{BNP_{O\text{-}O}}]_t \quad \text{(S16)}$$

$$Abs_{620} = \varepsilon_{\mathrm{O\text{-}O},620}[\mathrm{BNP_{O\text{-}O}}]_t + \varepsilon_{\mathrm{O\text{-}O},620}[{}^*\mathrm{BNP_{O\text{-}O}}]_t \quad \text{(S17)}$$

A snapshot of the code used to generate plots of absorbance as a function of time from the kinetic model is shown below in Figure S8. All of the estimated rate constants and parameters used to model time-dependent concentration and absorption are summarized in Table S1 and discussed individually in detail below.

```
mech = ParametricNDSolve[{
    cc'[t] == -k13 * cc[t] + k21 * oc[t] - k12 * cc[t],
    oc'[t] == k32 * oo[t] - k23 * oc[t] - k21 * oc[t] + k12 * cc[t],
    oo'[t] == k13 * cc[t] - k32 * oo[t] + k23 * oc[t] - kc * oo[t],
    d'[t] == kc * oo[t] - k32 * d[t],
    e'[t] == k32 * d[t] - k21 * e[t],
    f'[t] == k21 * e[t],
    cc[0] == cc0,
    oc[0] == oc0,
    oo[0] == 0,
    d[0] == 0,
    e[0] == 0,
    f[0] == 0},
   {cc, oc, oo, d, e, f},
   {t, 0, 1000}, {k13, k21, k12, k32, k23, kc, cc0, oc0}];
```

In[15]:=

```
Manipulate[
 Plot[Evaluate[{0.026 * oc[k13, k21, k12, k32, k23, kc, cc0, oc0][t] + 0.026 * e[k13, k21, k12, k32, k23, kc, cc0, oc0][t] +
      0.030 * oo[k13, k21, k12, k32, k23, kc, cc0, oc0][t] + 0.030 * d[k13, k21, k12, k32, k23, kc, cc0, oc0][t],
     0.023 * oo[k13, k21, k12, k32, k23, kc, cc0, oc0][t] + 0.023 * d[k13, k21, k12, k32, k23, kc, cc0, oc0][t]} /. mech],
  {t, 0, 100},
  LabelStyle → Directive[Black, Medium, "Arial", 14],
  AxesLabel → {"Time (min)", "Absorbance"},
  AspectRatio → 1,
  PlotLabels → Placed[{"460 nm", "620 nm"}, {Above}],
  PlotStyle → {{lightblue, Thickness[0.008]}, {Black, Thickness[0.008]}}],
 {k13, 0, 0.5}, {k21, 0, 0.5}, {k12, 0, 0.5}, {k32, 0, 0.5}, {k23, 0, 0.5}, {kc, 0, 0.5}, {cc0, 0, 100}, {oc0, 0, 100}]
```

Figure S8. Code used to plot time-dependent absorbance from the kinetic model in Wolfram Mathematica 12.[11,12]

Table S1. Summary of parameters used to model time-dependent absorbance and concentration for all polymers.

							Absorbance Plots	**Concentration Plots**		
	k_{13} (min^{-1})	k_{23} (min^{-1})	k_{32} (min^{-1})	k_{21} (min^{-1})	k_c (min^{-1})	Ω	$[BNP_{C\text{-}C}]_{t=0,abs}$ (μM)	$[BNP_{C\text{-}C}]_{t=0}$ (μM)	$[BNP_{O\text{-}C}]_{t=0}$ (μM)	$[BNP_{O\text{-}C}]_{t=0}$ (μM) (*residual*)
BNP-PMA$_{22}$	0.003	0.003	0.03	0.01	0	0.11	10	9.71	0.29	2.39
BNP-PMA$_{40}$	0.007	0.007	0.03	0.01	0.0022	0.28	14	13.62	0.38	0.97
BNP-PMA$_{53}$	0.017	0.017	0.03	0.01	0.0093	0.20	7.5	7.30	0.20	0.81
BNP-PMA$_{73}$	0.03	0.03	0.03	0.01	0.020	0.33	9.0	8.70	0.30	0.62
BNP-PMA$_{98}$	0.045	0.045	0.03	0.01	0.034	0.39	8.0	7.76	0.24	0.38
BNP-PMA$_{165}$	0.15	0.15	0.03	0.01	0.070	0.47	5.7	5.47	0.23	0.26
BNP-PMA$_{330}$	0.30	0.30	0.03	0.01	0.16	0.68	4.1	3.94	0.16	0.08

Determination of parameters for the kinetic model

Scheme S4. Thermal electrocyclization reactions of $BNP_{O\text{-}O}$ and $BNP_{O\text{-}C}$.

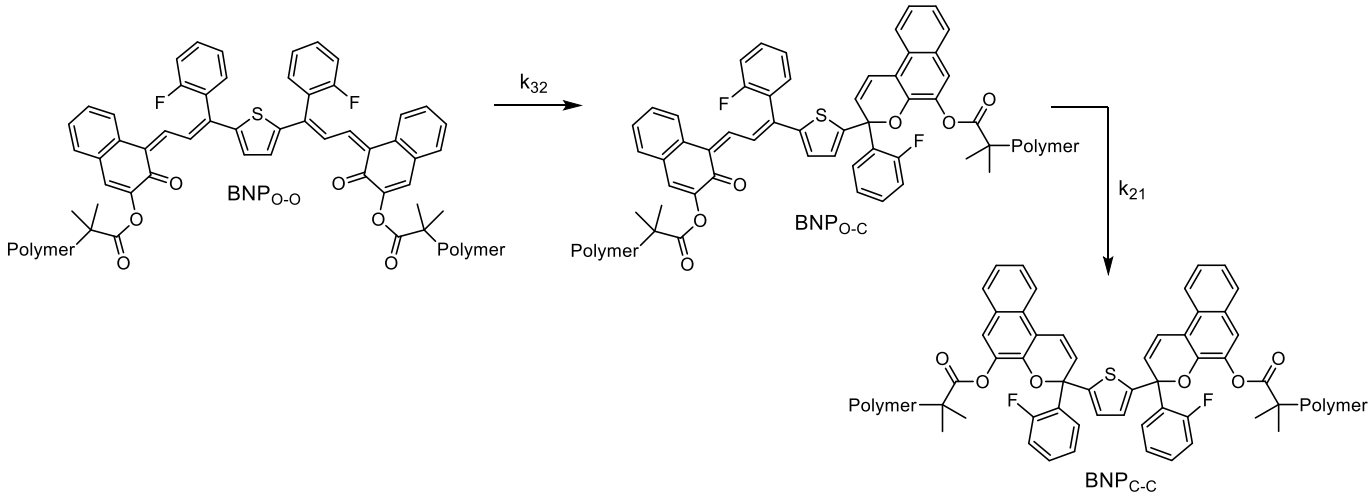

Rates of thermal electrocyclization. Values of k_{32} and k_{21} were determined from thermal fading experiments performed on **BNP-PMA$_{330}$** following either mechanochemical activation or photochemical activation. Values of k_{32} and k_{21} were determined from each experiment and averaged to provide the values of the rate constants used in the model. Following photochemical or mechanochemical activation as described above, the light source and sonication were turned off (t = 0) and absorbance data was collected. No other conditions were changed from those of the activation experiments. The rate equations describing the thermal ring-closing processes shown in Scheme S4 are given by equations S18 and S19 for the concentration of merocyanine species:

$$\frac{d[\mathrm{BNP_{O\text{-}O}}]_t}{dt} = -k_{32}[\mathrm{BNP_{O\text{-}O}}]_t \tag{S18}$$

$$\frac{d[\mathrm{BNP_{O\text{-}C}}]_t}{dt} = k_{32}[\mathrm{BNP_{O\text{-}O}}]_t - k_{21}[\mathrm{BNP_{O\text{-}C}}]_t \tag{S19}$$

The *DSolve* function in Mathematica was used to analytically solve the integrated rate laws to model the time-dependent concentration of merocyanine species, which are provided as equations S20 and S21:

$$[\mathrm{BNP_{O\text{-}O}}]_t = [\mathrm{BNP_{O\text{-}O}}]_{t=0} * e^{-k_{32}t} \tag{S20}$$

$$[\mathrm{BNP_{O\text{-}C}}]_t =$$

$$\frac{[\mathrm{BNP_{O\text{-}C}}]_{t=0} * k_{21}e^{-k_{21}t} - ([\mathrm{BNP_{O\text{-}C}}]_{t=0} + [\mathrm{BNP_{O\text{-}O}}]_{t=0}) * k_{32}e^{-k_{21}t} + [\mathrm{BNP_{O\text{-}O}}]_{t=0} * k_{32}e^{-k_{32}t}}{k_{21} - k_{32}} \tag{S21}$$

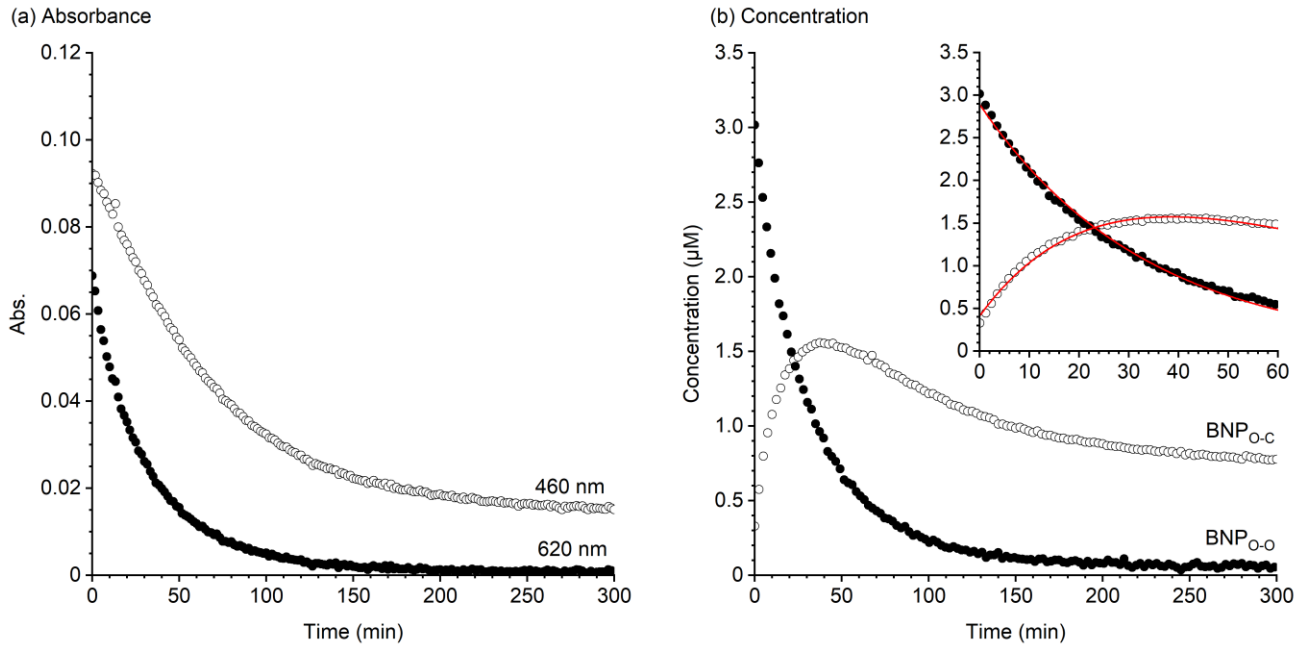

Figure S9. Determination of k_{32} and k_{21} from (a) absorbance and (b) concentration data acquired for thermal fading of BNP_{O-C} and BNP_{O-O} after mechanical activation of **BNP-PMA$_{330}$** and cessation of sonication. Time-dependent concentration curves were fitted to equations S20 and S21 (inset) to calculate values of k_{32} and k_{21}.

The absorbance data measured for the thermal electrocyclization of mechanochemically activated **BNP-PMA$_{330}$** are shown in Figure S9. The time-dependent absorbance data was converted to concentration of BNP_{O-C} and BNP_{O-O} and the first 60 minutes of data were fitted to equations S20 and S21 to obtain k_{32} and k_{21}. The same procedure was performed on the photochemically activated sample, and the average values of k_{32} and k_{21} from these experiments were determined to be 0.03 min^{-1} and 0.01 min^{-1}, respectively.

As shown in Figure S9b, after sonication is stopped, the concentration of BNP_{O-O} decreases as it is converted to BNP_{O-C}. Consequently, the concentration of BNP_{O-C} increases initially and then subsequently decreases as it is converted to BNP_{C-C}. However, in contrast to BNP_{O-O} which is ultimately completely converted to BNP_{O-C}, the concentration of BNP_{O-C} decreases more slowly at later times. This observation is consistent with previous studies of similar merocyanine dyes that identify different rates of thermal ring-closure for different merocyanine isomers, with the trans-cis isomer of the merocyanine species fading faster than the trans-trans isomer.[8,9] The generation of some slow fading trans-trans BNP_{O-C} species would account for the small fraction of the absorbance at 460 nm that is persistent on the time scale of the reaction. The trans-cis and trans-trans isomers of similar BNP_{O-C} species have nearly identical absorption spectra, making it difficult to differentiate the two compounds spectroscopically. Because we do not account for isomerization in the kinetic model, the measured value of k_{21} that we employ in the model only captures the fast fading component of BNP_{O-C} and the slow fading fraction is neglected. Despite this simplification, the kinetic model aligns well with the experimental data and reflects the time-dependent changes in absorbance and merocyanine concentration.

Determination of rates of ring-opening. After defining k_{32} and k_{21} in the model, the values of k_{13} and k_{23} for each polymer were determined empirically by adjusting the parameters, along with $[BNP_{C\text{-}C}]_{t=0,abs}$, until the predicted values of B_{620} and B_{460} were consistent with average values determined experimentally. For the purposes of the model, we assume that k_{13} and k_{23} are equal. Figure S1 demonstrates that a small amount of $BNP_{O\text{-}C}$ present at the start of the reaction is immediately lost, indicating that $BNP_{O\text{-}C}$ is converted mechanochemically to $BNP_{O\text{-}O}$. The rate of ring-opening is dependent upon the force applied to the mechanophore, and thus the length of the polymer chains attached to the mechanophore. Therefore, we assume that upon thermal electrocyclization of $BNP_{O\text{-}O}$ to $BNP_{O\text{-}C}$, the rate of reactivation and associated rate constant k_{23}, will be approximately equal to the original forward rate of ring-opening described by k_{13}, since the length of the polymer chains attached to the mechanophore is the same. Not all polymer chains in solution react under ultrasonication,[13] so the boundary condition $[BNP_{C\text{-}C}]_{t=0,abs}$ reflects the concentration of polymer that is activated, rather than the total concentration of polymer in solution. All other initial concentrations were set to zero to model time-dependent changes in absorption, consistent with our treatment of the experimental absorbance data.

Determination of chain scission rates. The rate of polymer chain scission induced by ultrasonication is typically determined from changes in molecular weight averages measured by GPC.[3] However, rates determined by this method are not comparable to rates determined spectroscopically.[13] Accordingly, the rate constant for polymer chain cleavage, k_c, was first estimated for **BNP-PMA$_{165}$** by adjusting the parameter so that the model reflected the experimental data at extended sonication times (see Figure S19). This value of k_c was then used to determine a scaling factor so that previously reported relationships for the molecular-weight-dependent rate of polymer chain scission measured by GPC could be converted to appropriate values for the kinetic model. We derived eq S22 based on reported chain cleavage rates of PMA by Kryger et al. [3] Using this relationship, we then calculated the estimated rate constant for chain cleavage based on GPC measurements, $k_{c,GPC}$, expected for each polymer in our study (Table S2). We note that these rate constants have units of min^{-1} kDa^{-1} and must be multiplied by the molecular weight of the polymer repeat unit, M_o (for PMA, M_o = 0.0861 kg/mol). A scaling factor of 8150 was then determined by dividing the value of k_c determined for **BNP-PMA$_{165}$** by the corresponding calculated value of $k_{c,GPC}$. This scaling factor was used to convert calculated values of $k_{c,GPC}$ (with units of min^{-1}) for each polymer of varying molecular weight to appropriate values of k_c to be used in the kinetic model.

$$k_{c,GPC} = 7.73 \times 10^{-7} * M_n - 2.78 \times 10^{-5} \quad (S22)$$

Table S2. Molecular-weight-dependent rate constants for polymer chain scission.

Molecular Weight (M_n, kDa)	$k_{c,GPC}$ calculated from eq S22 (min^{-1} kDa^{-1})	$M_o * k_{c,GPC}$ (min^{-1})	k_c ($8150 * M_o * k_{c,GPC}$) (min^{-1})
22	0	0	0
40	3.1×10^{-6}	2.7×10^{-7}	0.0022
53	1.3×10^{-5}	1.1×10^{-6}	0.0093
73	2.9×10^{-5}	2.5×10^{-6}	0.020
98	4.8×10^{-5}	4.1×10^{-6}	0.034
165	1.0×10^{-4}	8.6×10^{-6}	0.070
330	2.3×10^{-4}	2.0×10^{-5}	0.16

Initial concentrations in the time-dependent concentration kinetic model. A small amount of $BNP_{O\text{-}C}$ is present in solution prior to ultrasound-induced mechanochemical activation of each polymer. In order to monitor changes in absorbance resulting from mechanochemical activation of the BNP mechanophore, the absorbance at *t*=0 was subtracted from the time-dependent absorbance values as described above. However, it is useful to characterize the concentration of merocyanine species at any point in the reaction, and therefore this step was omitted when converting time-dependent absorbance to concentration of $BNP_{O\text{-}C}$ and $BNP_{O\text{-}O}$. In order to account for this in the kinetic model, the initial fractional concentration of polymer that is activated during sonication (% activation, Ω) was calculated from the empirically determined values of $[BNP_{C\text{-}C}]_{t=0,abs}$ identified from the time-dependent absorbance models relative to the total concentration of polymer in solution according to eq S23:

$$\Omega = \frac{[\mathrm{BNP_{C\text{-}C}}]_{t=0,abs}}{[\mathrm{polymer}]} \tag{S23}$$

Only a fraction of the polymer chains subjected to sonication reacts. Likewise, only a portion of $BNP_{O\text{-}C}$ present at the start of ultrasonication is expected to contribute to the dynamic equilibrium. This fractional concentration of active $BNP_{O\text{-}C}$, $[\mathrm{BNP_{O\text{-}C}}]_{t=0}$, is defined according to eq S24 with respect to the concentration of $BNP_{O\text{-}C}$ determined from the experimental data, $[\mathrm{BNP_{O\text{-}C}}]_{t=0,observed}$. The residual $BNP_{O\text{-}C}$ that is present in the reaction but does not become activated is defined according to eq S25. This quantity was determined for each polymer and added as a constant to the calculated concentration of $BNP_{O\text{-}C}$ in each time-dependent concentration model. The fractional concentration of active $BNP_{C\text{-}C}$ at *t*=0 was finally calculated according to eq S26. The values of all parameters that were used in the kinetic model are presented in Table S1.

$$[\mathrm{BNP_{O\text{-}C}}]_{t=0} = \Omega * [\mathrm{BNP_{O\text{-}C}}]_{t=0,observed} \tag{S24}$$

$$[\mathrm{BNP_{O\text{-}C}}]_{t=0,residual} = (1-\Omega) * [\mathrm{BNP_{O\text{-}C}}]_{t=0,observed} \tag{S25}$$

$$[\mathrm{BNP_{C\text{-}C}}]_{t=0} = \Omega * [\mathrm{Polymer}] - [\mathrm{BNP_{O\text{-}C}}]_{t=0} \tag{S26}$$

$BNP_{O\text{-}C}$ and $^*BNP_{O\text{-}C}$, as well as $BNP_{O\text{-}O}$ and $^*BNP_{O\text{-}O}$, are spectroscopically indistinguishable. Thus, the relationships presented in eq S27 and S28 were used to plot the modeled time-dependent concentration of each merocyanine species relative to the total concentration of polymer:

$$\frac{[\mathrm{BNP_{O\text{-}C}}]_{t,apparent}}{[\mathrm{polymer}]} = \frac{[\mathrm{BNP_{O\text{-}C}}]_t + [^*\mathrm{BNP_{O\text{-}C}}]_t}{[\mathrm{polymer}]} \tag{S27}$$

$$\frac{[\mathrm{BNP_{O\text{-}O}}]_{t,apparent}}{[\mathrm{polymer}]} = \frac{[\mathrm{BNP_{O\text{-}O}}]_t + [^*\mathrm{BNP_{O\text{-}O}}]_t}{[\mathrm{polymer}]} \tag{S28}$$

Results of kinetic modeling

Experimentally measured time-dependent absorbance at 460 and 620 nm and the corresponding data for the concentration of $BNP_{O\text{-}C}$ and $BNP_{O\text{-}O}$ as a function of sonication time is shown below and compared directly to the results of the kinetic model for each polymer (Figures S10–S16). The kinetic model closely reproduces the experimental results for the force-dependent mechanochemical activation of bis-naphthopyran supporting the proposed mechanism.

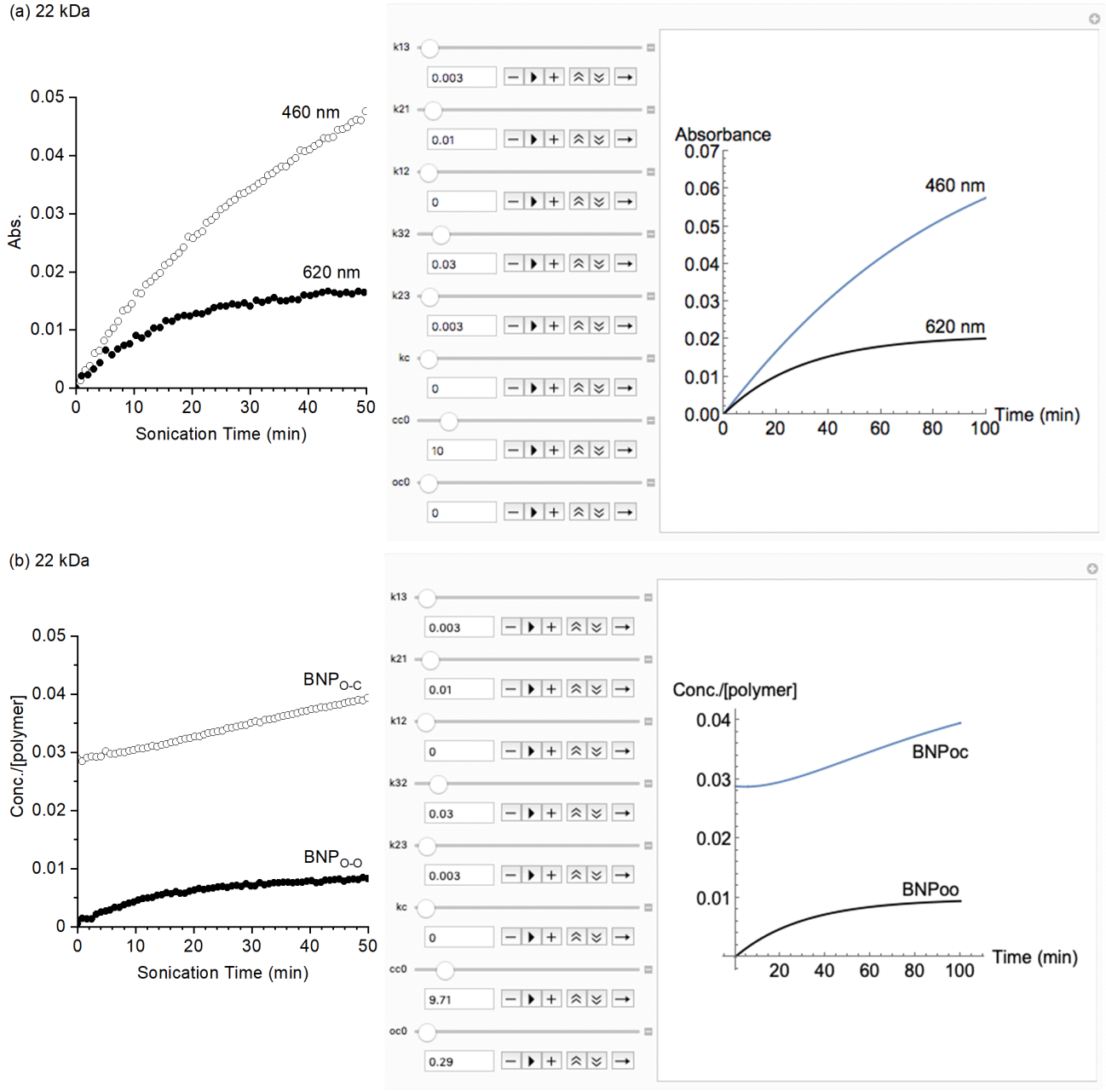

Figure S10. Time-dependent (a) absorbance at 460 and 620 nm, and (b) concentration of $BNP_{O\text{-}C}$ and $BNP_{O\text{-}O}$ for the mechanochemical activation of **BNP-PMA$_{22}$**. Experimental data (*left*) is compared to results from the kinetic model (*right*).

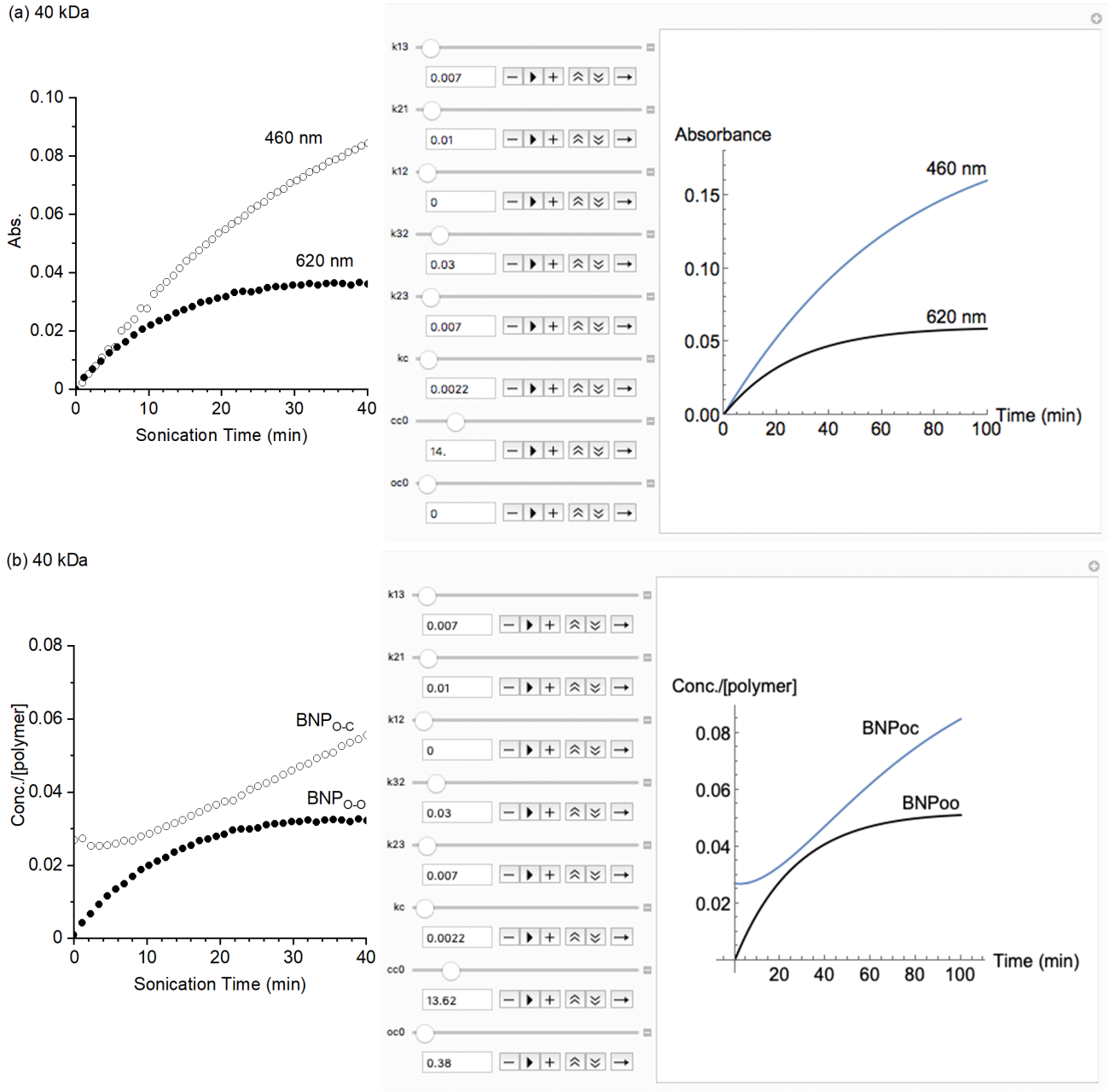

Figure S11. Time-dependent (a) absorbance at 460 and 620 nm, and (b) concentration of BNP_{O-C} and BNP_{O-O} for the mechanochemical activation of **BNP-PMA$_{40}$**. Experimental data (*left*) is compared to results from the kinetic model (*right*).

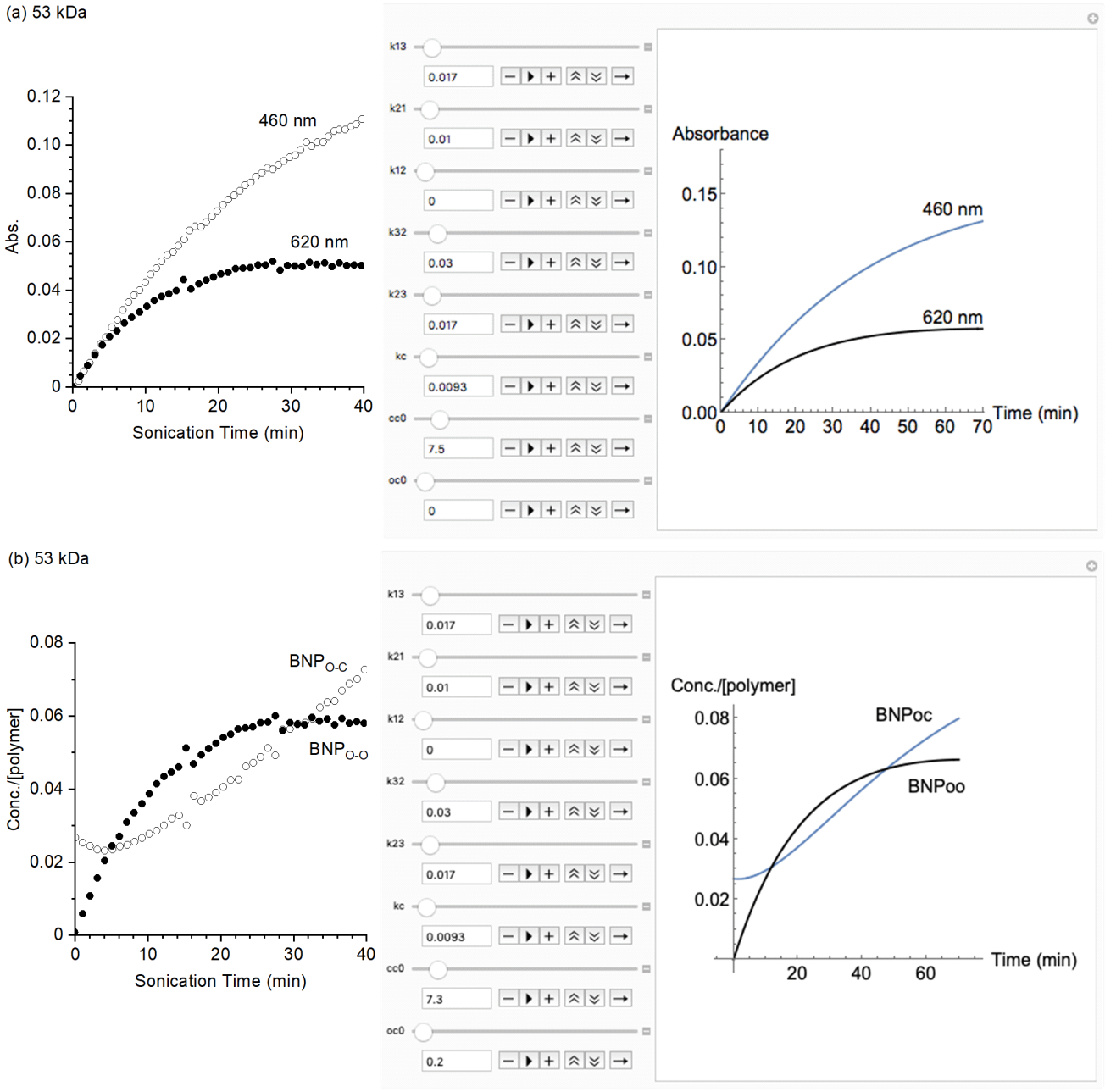

Figure S12. Time-dependent (a) absorbance at 460 and 620 nm, and (b) concentration of BNP_{O-C} and BNP_{O-O} for the mechanochemical activation of **BNP-PMA$_{53}$**. Experimental data (*left*) is compared to results from the kinetic model (*right*).

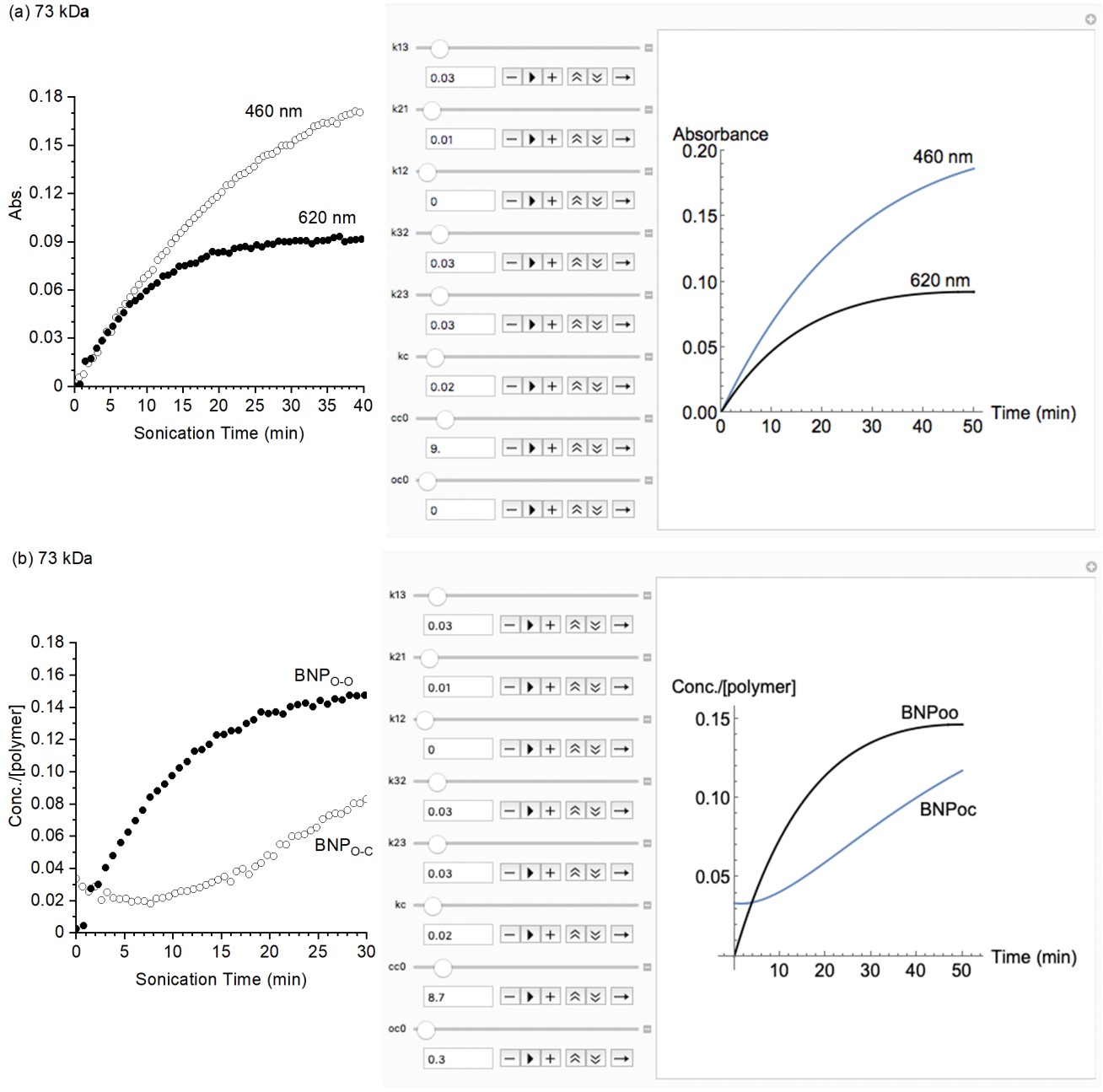

Figure S13. Time-dependent (a) absorbance at 460 and 620 nm, and (b) concentration of BNP_{O-C} and BNP_{O-O} for the mechanochemical activation of **BNP-PMA$_{73}$**. Experimental data (*left*) is compared to results from the kinetic model (*right*).

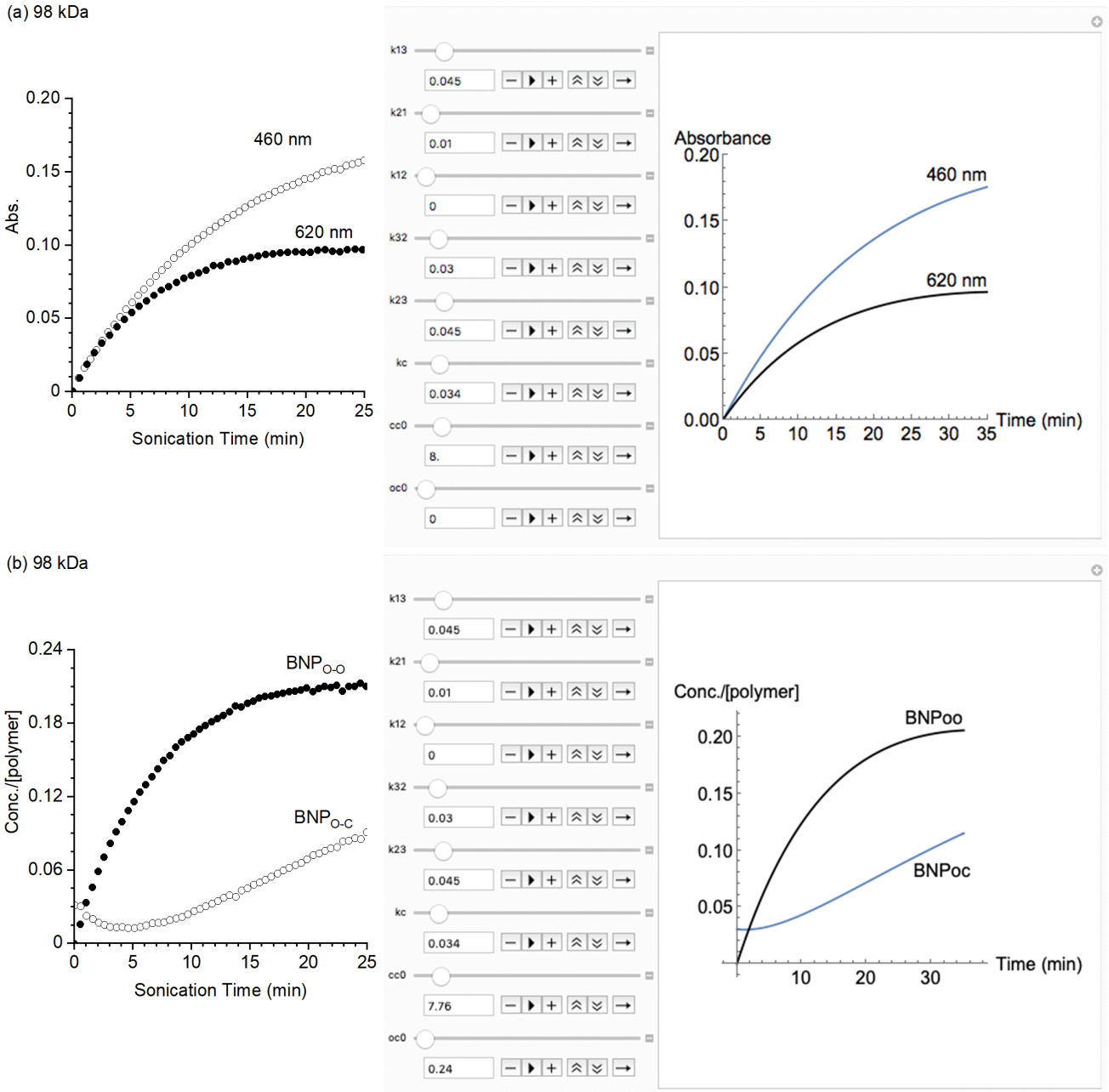

Figure S14. Time-dependent (a) absorbance at 460 and 620 nm, and (b) concentration of $BNP_{O\text{-}C}$ and $BNP_{O\text{-}O}$ for the mechanochemical activation of **BNP-PMA$_{98}$**. Experimental data (*left*) is compared to results from the kinetic model (*right*).

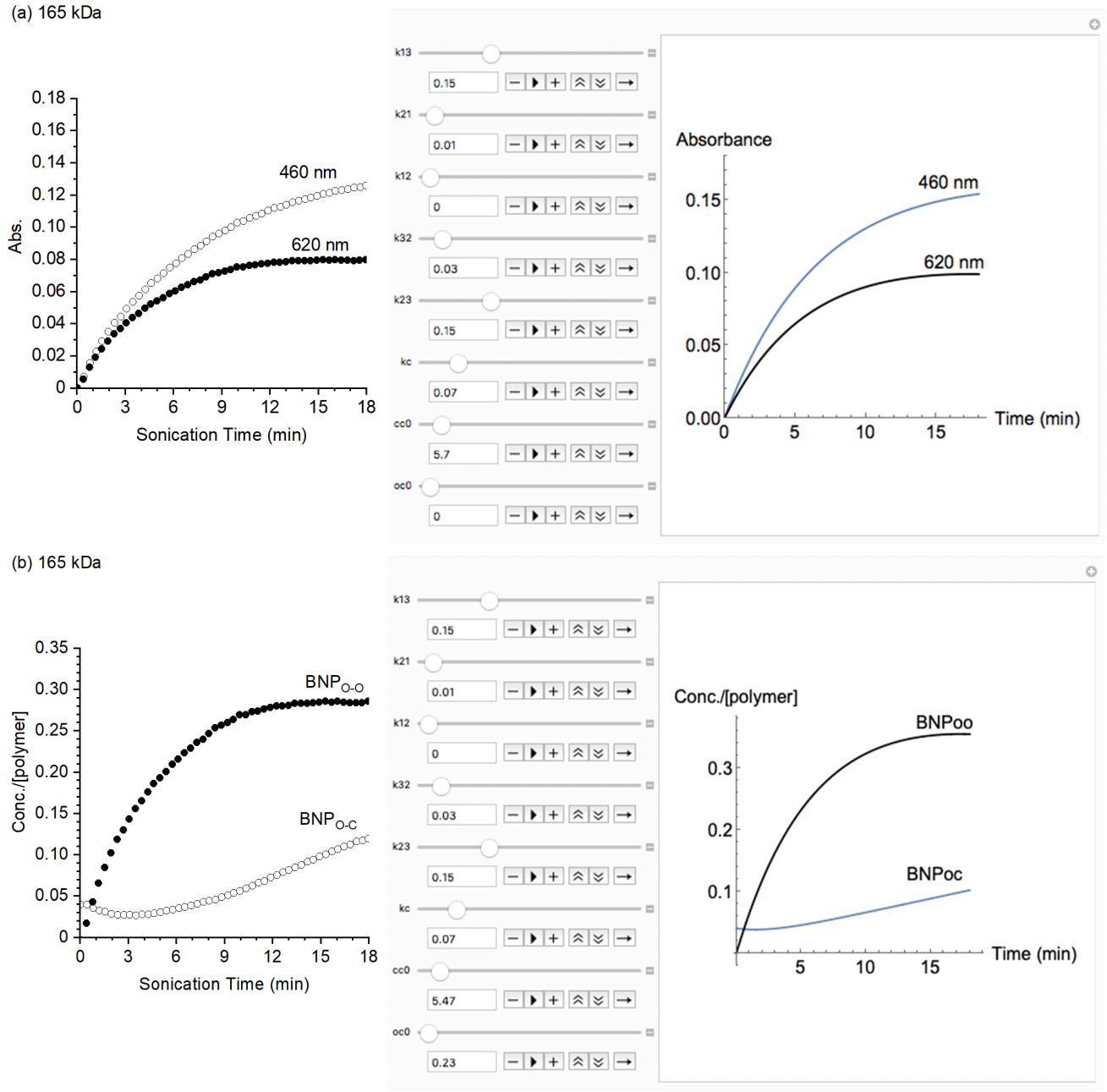

Figure S15. Time-dependent (a) absorbance at 460 and 620 nm, and (b) concentration of BNP_{O-C} and BNP_{O-O} for the mechanochemical activation of **BNP-PMA$_{165}$**. Experimental data (*left*) is compared to results from the kinetic model (*right*).

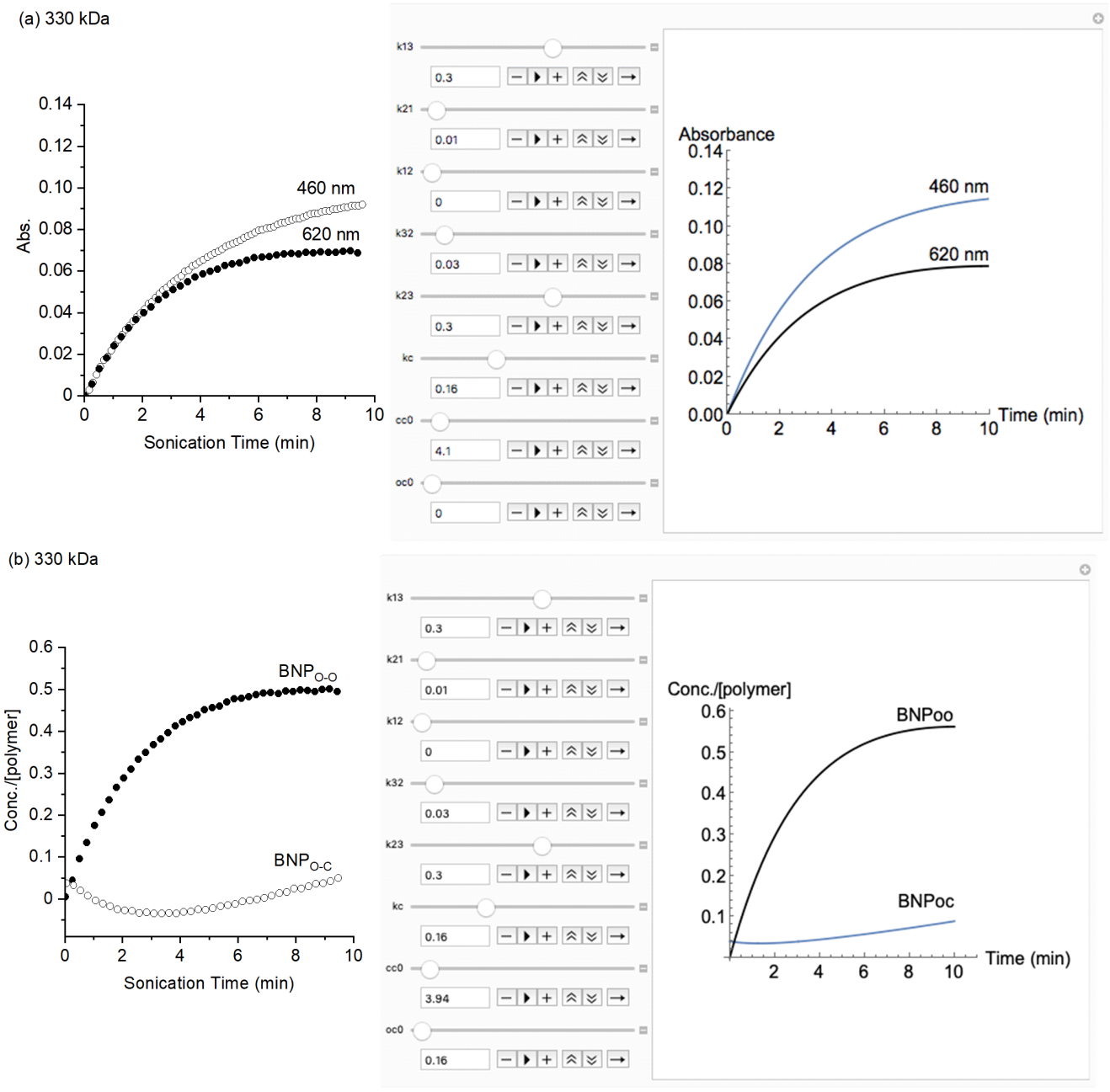

Figure S16. Time-dependent (a) absorbance at 460 and 620 nm, and (b) concentration of BNP_{O-C} and BNP_{O-O} for the mechanochemical activation of **BNP-PMA$_{330}$**. Experimental data (*left*) is compared to results from the kinetic model (*right*).

Effect of polymer chain scission. Chain scission occurs for polymers subjected to ultrasonication. We demonstrate below that the kinetic model closely reproduces the experimental data when chain scission is explicitly included and that the effect of chain scission on the value of B_{620}/B_{460} is minimal. **BNP-PMA$_{22}$**, **BNP-PMA$_{98}$**, and **BNP-PMA$_{165}$** presenting a large range of molecular weights were subjected to extended ultrasonication treatment for 150, 65, and 70 min respectively (Figures S17–S19). Changes in molecular weight for these polymers at various sonication times were characterized by GPC (Table S3).

Table S3. Molecular weight (M_n) and dispersity measured by GPC-MALLS for polymers after ultrasonication.

	BNP-PMA$_{22}$	**BNP-PMA$_{98}$**		**BNP-PMA$_{165}$**
Sonication Time (min)	85	17	31	23
***M*$_n$ (kDa)**	21	78	55	78
Đ	1.18	1.16	1.24	1.21

Ultrasonication of **BNP-PMA$_{22}$** for extended time results in negligible chain scission. The molecular weight and dispersity of the polymer is unchanged after 85 minutes of sonication. Furthermore, the time-dependent absorbance and associated concentration data shows that the concentration of BNP$_{O\text{-}O}$ reaches a constant value that is maintained for the duration of the sonication experiment, consistent with the absence of irreversible degradation caused by chain cleavage (Figure S17). These results for the mechanochemical activation of **BNP-PMA$_{22}$** demonstrate that chain scission is not required for the system to reach a mechanostationary state.

Extended ultrasound-induced mechanical activation of higher molecular weight **BNP-PMA$_{98}$** and **BNP-PMA$_{165}$** results in appreciable amounts of chain scission as expected. The molecular weight of **BNP-PMA$_{98}$** is reduced to 78 kDa after 17 min and 55 kDa after 31 min of sonication. **BNP-PMA$_{165}$** exhibits a faster rate of chain cleavage. After 23 min of sonication, the molecular weight was reduced to 78 kDa. Nevertheless, the experimental results for the mechanochemical reaction are reliably captured by the kinetic model when chain scission is explicitly included (Figure S18 and S19).

The impact of chain cleavage on the outcome of mechanochemical activation of each polymer and its effect on the ratio of B_{620}/B_{460} was investigated by comparing time-dependent absorbance plots generated from the kinetic model that include and omit the chain scission parameter (Figures S20–S26). Time-dependent absorbance traces for both mechanisms were modeled for each polymer and their corresponding values of B_{620}/B_{460} were calculated. In Figures S21–S26, a model that explicitly incorporates chain cleavage is shown on the left using values of k_c from Table S1. The model that omits chain cleavage is displayed on the right ($k_c = 0$). This comparison demonstrates that while chain cleavage impacts how quickly the maximum absorbance values are reached and the rate at which irreversible degradation occurs, the value of B_{620}/B_{460} is not significantly affected.

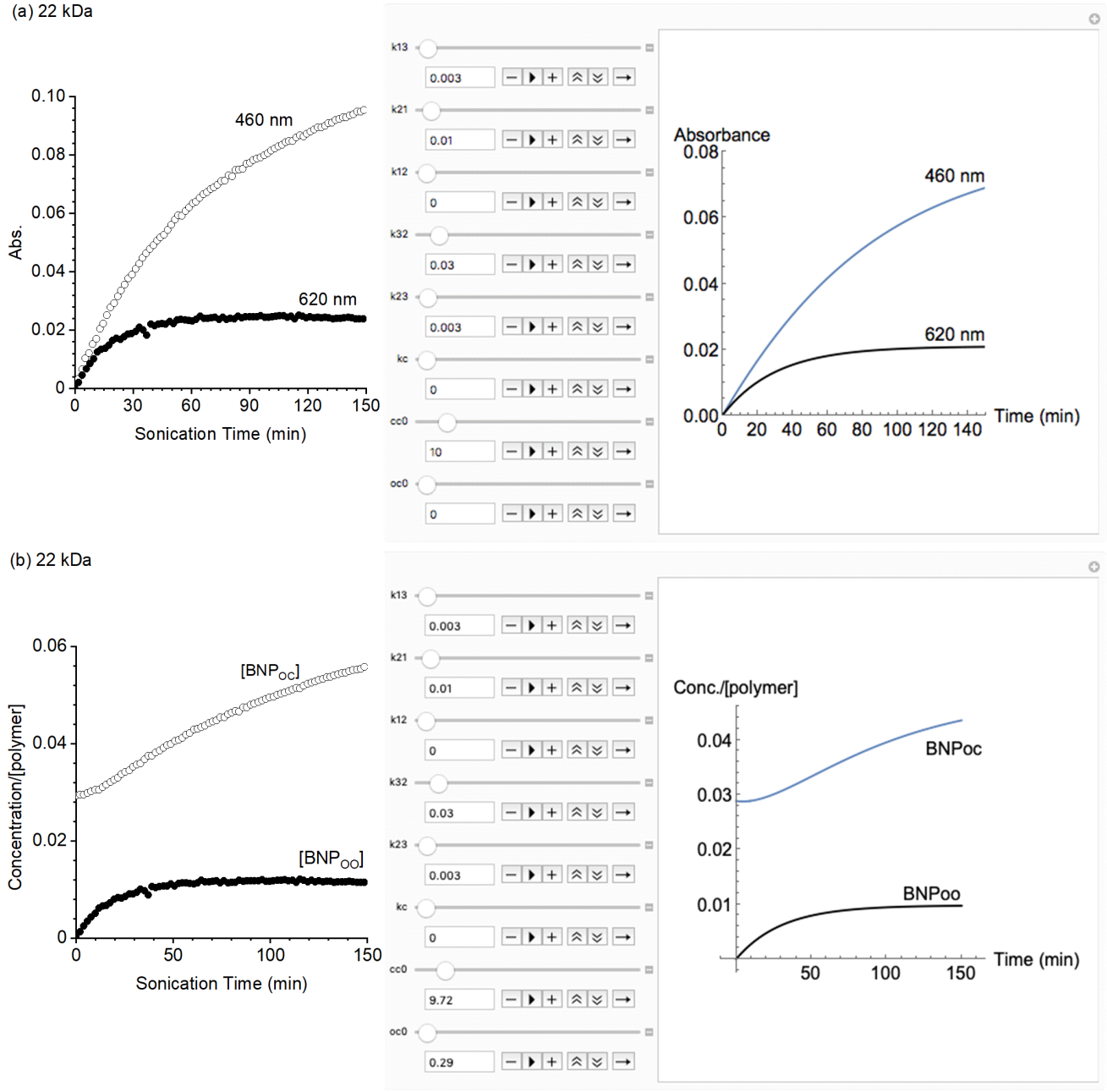

Figure S17. Time-dependent (a) absorbance at 460 and 620 nm, and (b) concentration of $BNP_{O\text{-}C}$ and $BNP_{O\text{-}O}$ for the mechanochemical activation of **BNP-PMA$_{22}$** for extended sonication time. Experimental data (*left*) is compared to results from the kinetic model (*right*).

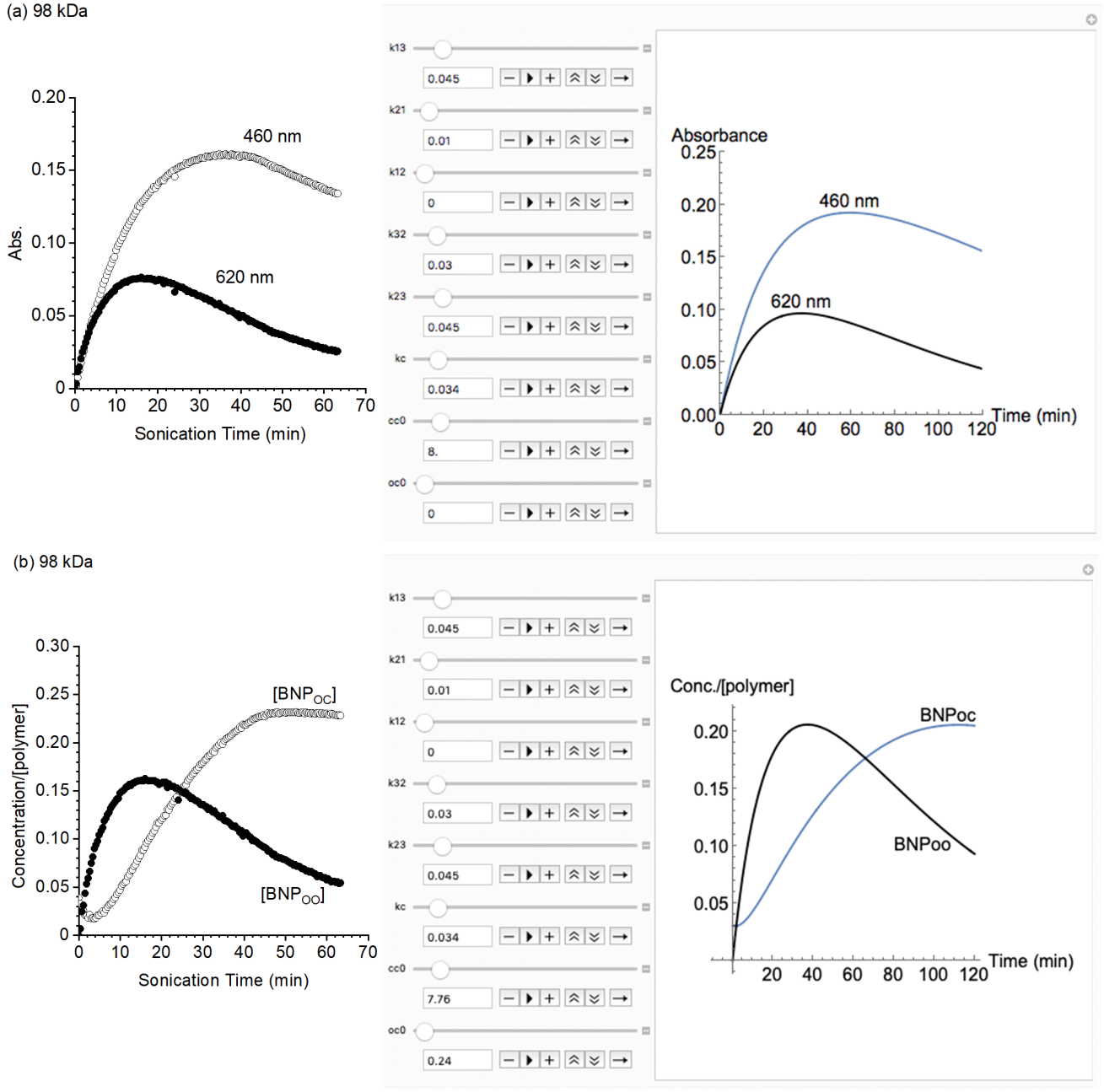

Figure S18. Time-dependent (a) absorbance at 460 and 620 nm, and (b) concentration of $BNP_{O\text{-}C}$ and $BNP_{O\text{-}O}$ for the mechanochemical activation of **BNP-PMA$_{98}$** for extended sonication time. Experimental data (*left*) is compared to results from the kinetic model (*right*).

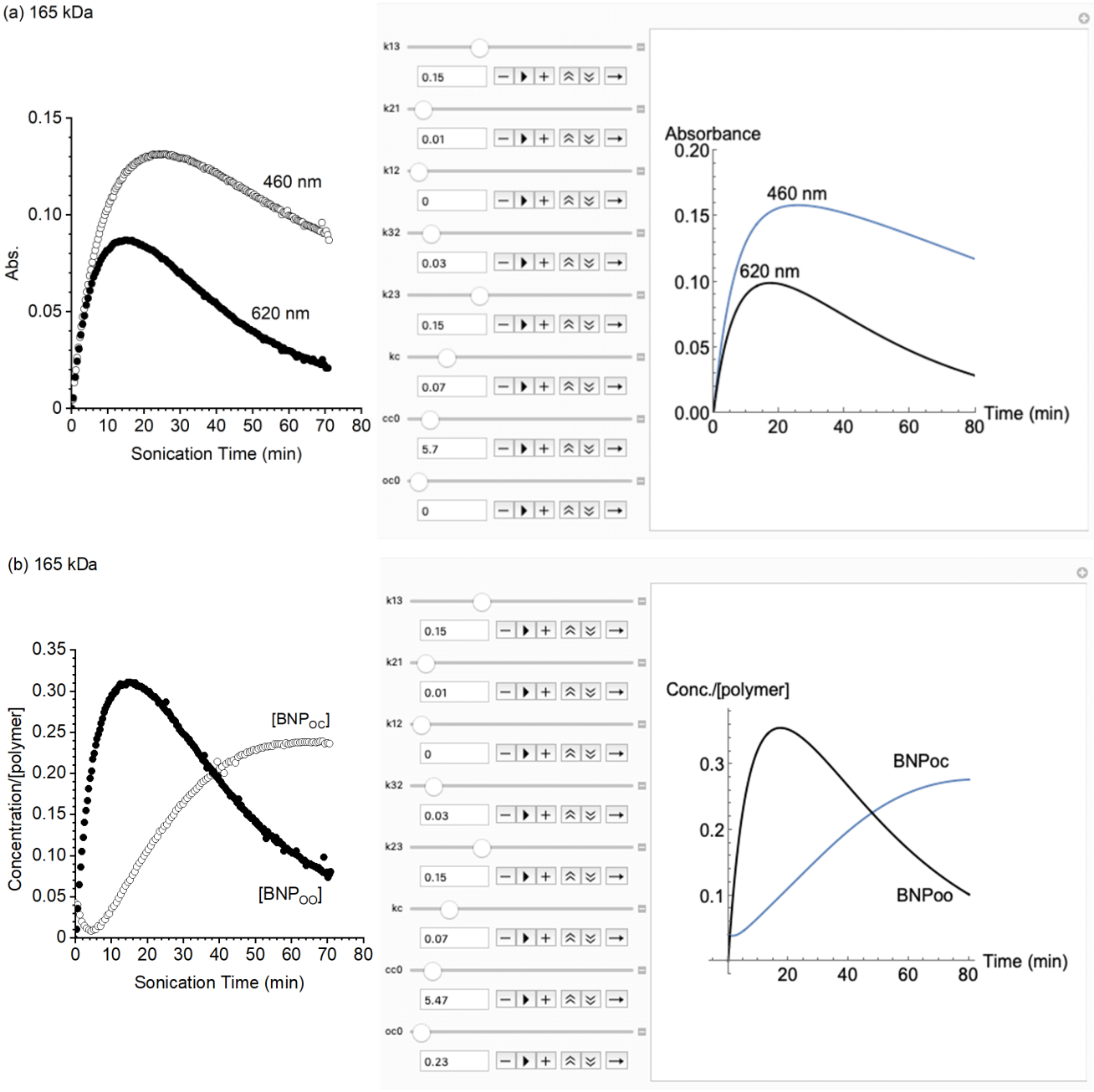

Figure S19. Time-dependent (a) absorbance at 460 and 620 nm, and (b) concentration of $BNP_{O\text{-}C}$ and $BNP_{O\text{-}O}$ for the mechanochemical activation of **BNP-PMA$_{165}$** for extended sonication time. Experimental data (*left*) is compared to results from the kinetic model (*right*).

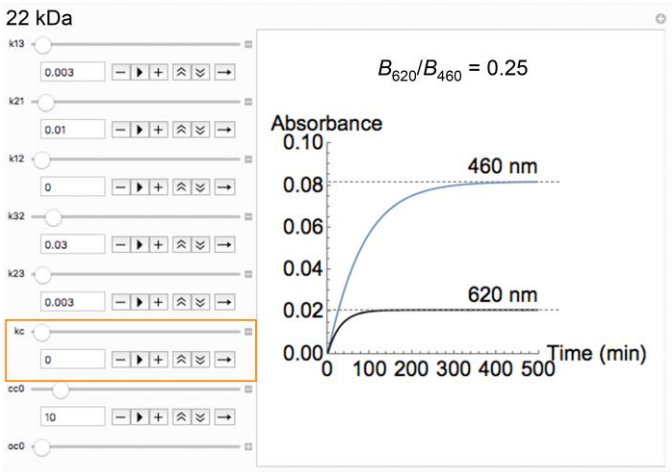

Figure S20. Comparison of the effect of chain cleavage on the values of B_{620}/B_{460} calculated from the kinetic model. Chain scission is not observed for sonication of **BNP-PMA$_{22}$**. The ratios of B_{620}/B_{460} predicted from the model closely match the experimentally determined values.

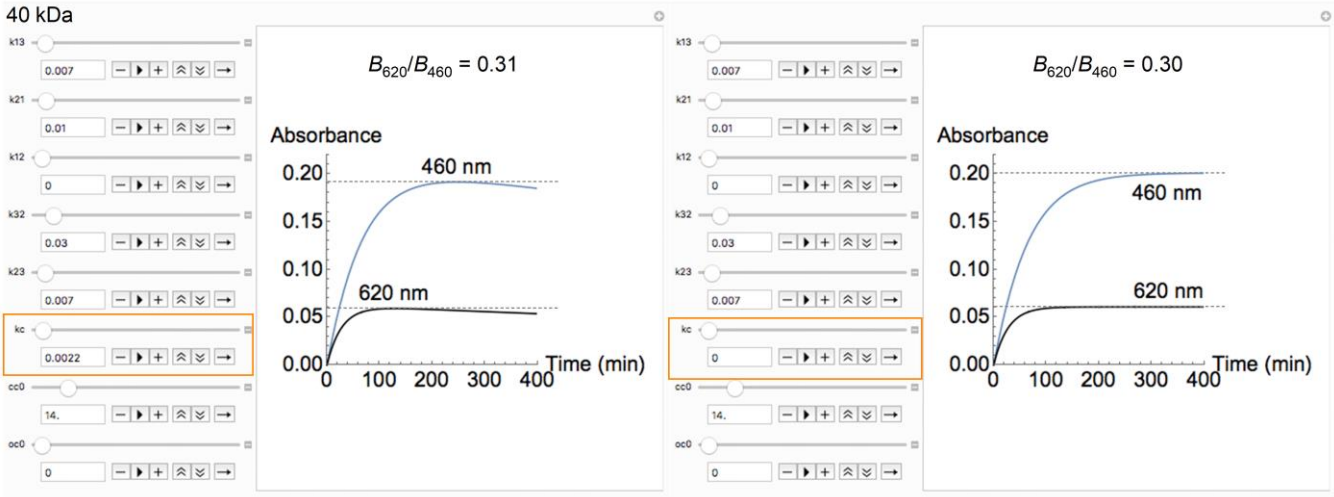

Figure S21. Comparison of the effect of chain cleavage on the values of B_{620}/B_{460} calculated for **BNP-PMA$_{40}$** from the kinetic model. The ratios of B_{620}/B_{460} predicted from the model closely match the experimentally determined values. Chain scission has a minimal impact on the value of B_{620}/B_{460}.

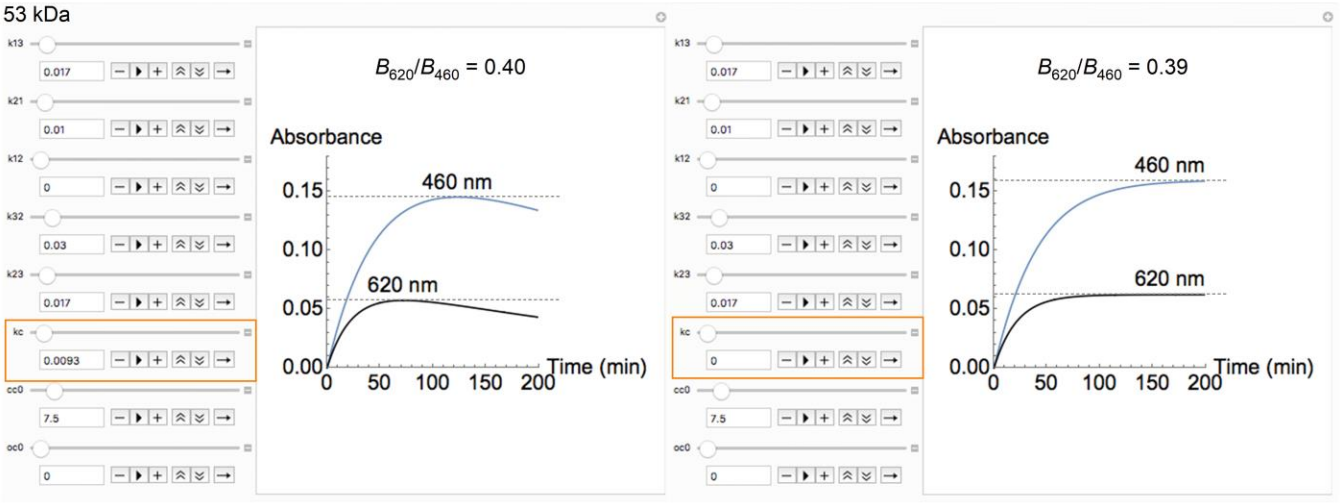

Figure S22. Comparison of the effect of chain cleavage on the values of B_{620}/B_{460} calculated for **BNP-PMA$_{53}$** from the kinetic model. The ratios of B_{620}/B_{460} predicted from the model closely match the experimentally determined values. Chain scission has a minimal impact on the value of B_{620}/B_{460}.

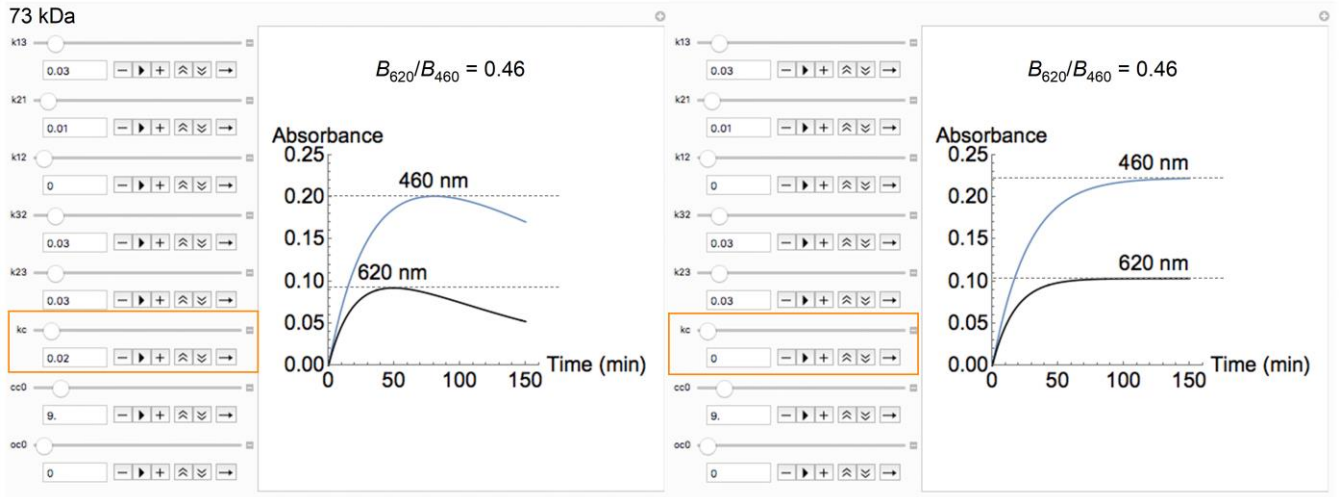

Figure S23. Comparison of the effect of chain cleavage on the values of B_{620}/B_{460} calculated for **BNP-PMA$_{73}$** from the kinetic model. The ratios of B_{620}/B_{460} predicted from the model closely match the experimentally determined values. Chain scission has a minimal impact on the value of B_{620}/B_{460}.

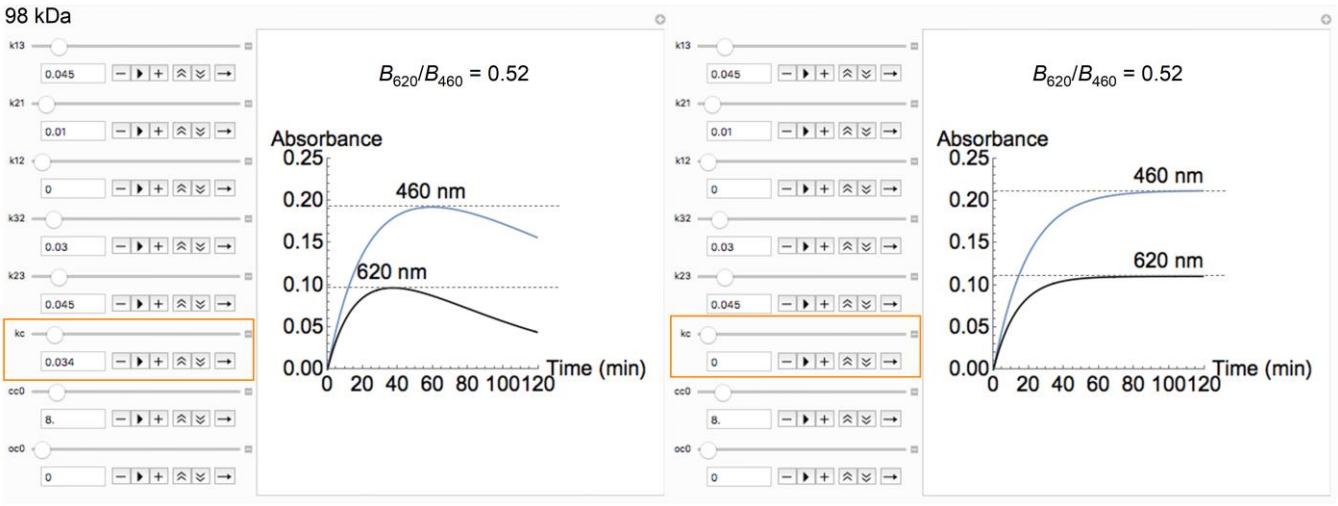

Figure S24. Comparison of the effect of chain cleavage on the values of B_{620}/B_{460} calculated for **BNP-PMA$_{98}$** from the kinetic model. The ratios of B_{620}/B_{460} predicted from the model closely match the experimentally determined values. Chain scission has a minimal impact on the value of B_{620}/B_{460}.

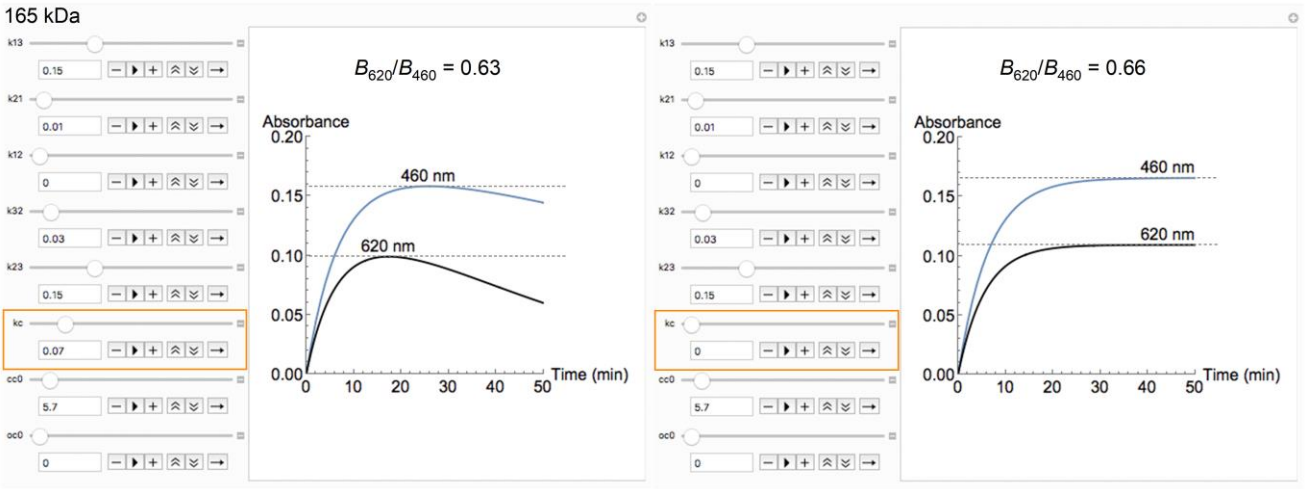

Figure S25. Comparison of the effect of chain cleavage on the values of B_{620}/B_{460} calculated for **BNP-PMA$_{165}$** from the kinetic model. The ratios of B_{620}/B_{460} predicted from the model closely match the experimentally determined values. Chain scission has a minimal impact on the value of B_{620}/B_{460}.

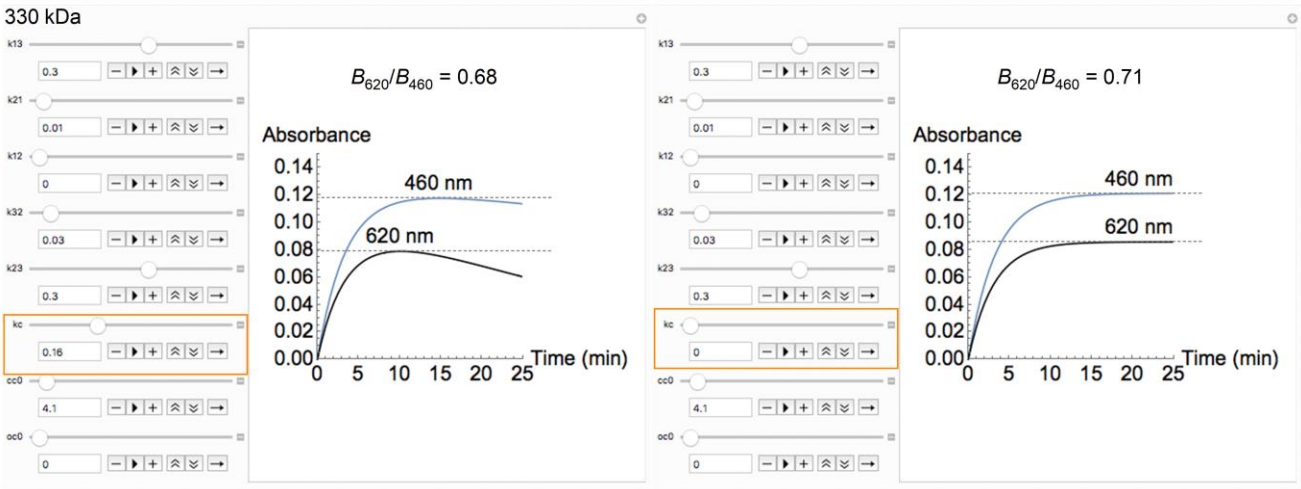

Figure S26. Comparison of the effect of chain cleavage on the values of B_{620}/B_{460} calculated for **BNP-PMA$_{330}$** from the kinetic model. The ratios of B_{620}/B_{460} predicted from the model closely match the experimentally determined values. Chain scission has a minimal impact on the value of B_{620}/B_{460}.

Analysis of the predicted effect of k_{12}. Experimental data and the results of kinetic modeling are consistent with a mechanism in which BNP$_{C\text{-}C}$ is converted directly to BNP$_{O\text{-}O}$. The experimentally observed formation of BNP$_{O\text{-}C}$ and BNP$_{O\text{-}O}$ under mechanical activation is mechanistically distinct from the sequential process observed from photochemical activation (see Figure S1).

To further investigate whether the formation of BNP$_{O\text{-}C}$ directly from BNP$_{C\text{-}C}$ was occurring (with corresponding rate constant k_{12}) to any significant extent with mechanical force, time-dependent concentrations of merocyanine products were compared to models in which k_{12} was either included or omitted (Figure S27). The concentration of BNP$_{O\text{-}C}$ present in solution prior to sonication is observed to decrease immediately upon initiating sonication, which manifests as a concave up region in the curve for the concentration of BNP$_{O\text{-}C}$ at early sonication times. This feature in the experimental data is replicated when k_{12} is omitted from the kinetic model. When the reaction pathway for the direct formation BNP$_{O\text{-}C}$ from BNP$_{C\text{-}C}$ is included in the model (with a non-zero value for k_{12}), this concave up feature is no longer observed. While a mechanism in which BNP$_{C\text{-}C}$ is first converted to BNP$_{O\text{-}C}$ followed by rapid conversion to BNP$_{O\text{-}O}$ cannot be completely ruled out, the results of the model indicate that k_{12} is either zero or very small compared to k_{23}. The time-dependent absorption and concentration data shows immediate generation of BNP$_{O\text{-}O}$ in all sonication experiments, in direct contrast to the photoactivation experiment in which BNP$_{O\text{-}C}$ is clearly generated first, followed by the production of BNP$_{O\text{-}O}$ (Figure S1).

It is also possible that a small fraction of chains is only able to convert BNP$_{C\text{-}C}$ to BNP$_{O\text{-}C}$, which cannot react further to generate BNP$_{O\text{-}O}$. This situation would arise if the force required, and thus the threshold chain length, for generating BNP$_{O\text{-}O}$ from BNP$_{O\text{-}C}$ is greater than that for conversion of BNP$_{C\text{-}C}$ to BNP$_{O\text{-}C}$. Importantly, however, differences in threshold chain length for mechanophores with varying reactivity are statistically small.[3] Therefore,

under this hypothetical mechanism, it is reasonable to expect that the majority of chains in solution that are long enough to be activated mechanochemically to form $BNP_{O\text{-}C}$ would also experience enough force to ultimately be converted to $BNP_{O\text{-}O}$. The features we observe in the experimental absorption data and the supporting evidence provided by the kinetic model are consistent with a dominant mechanism in which $BNP_{C\text{-}C}$ is effectively converted directly to $BNP_{O\text{-}O}$, and $BNP_{O\text{-}C}$ is generated via thermal electrocyclization.

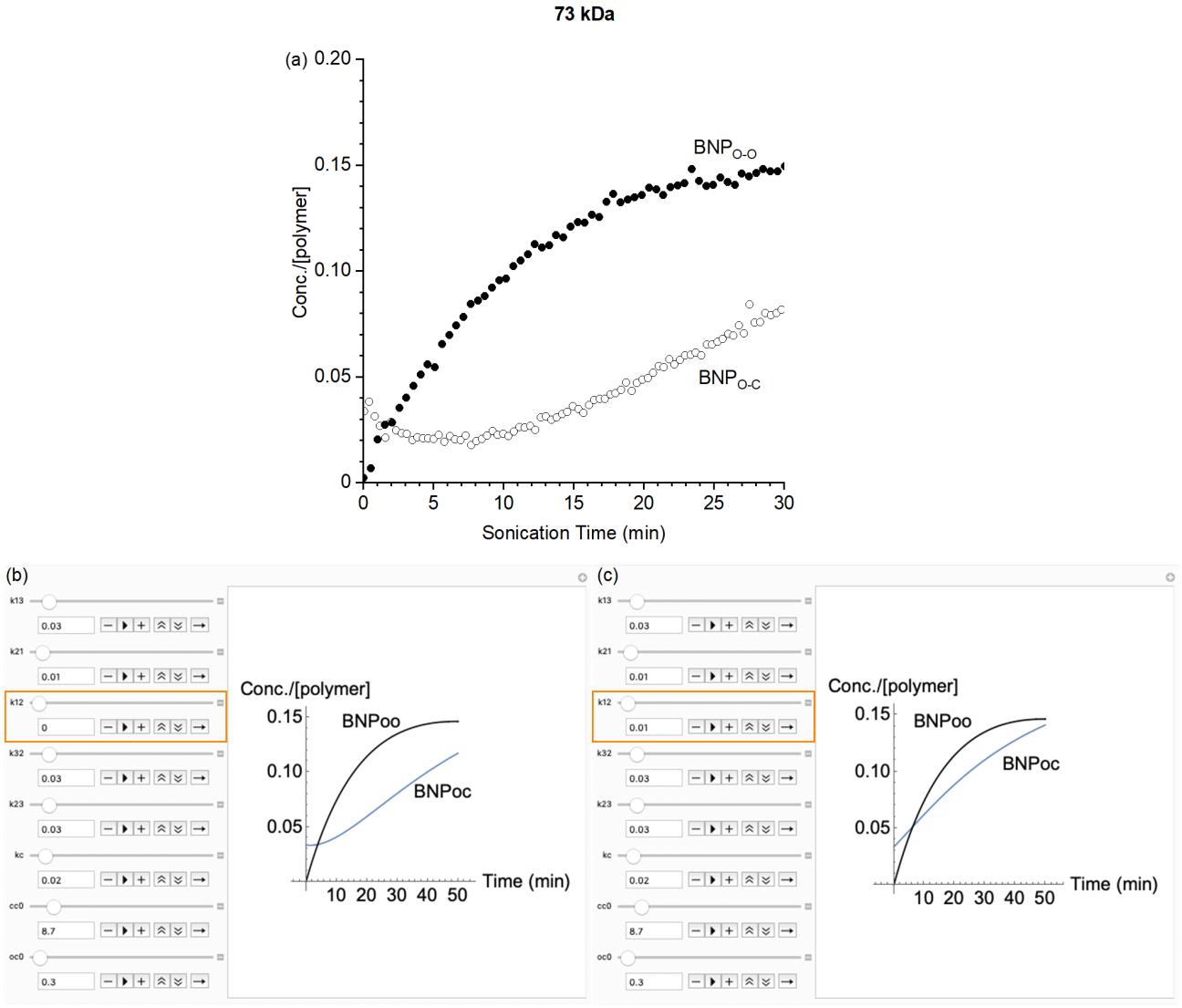

Figure S27. Comparison of the mechanochemical activation data acquired for **BNP-PMA$_{73}$** and the predicted effect of k_{12} from the kinetic model. (a) Concentration of merocyanine species as a function of sonication time, compared to results of the kinetic model (b) with k_{12} = 0 and (c) with k_{12} = 0.01 min^{-1}. The kinetic model suggests that the direct formation of $BNP_{O\text{-}C}$ from $BNP_{C\text{-}C}$, with associated rate constant k_{12}, is insignificant compared to the rate of conversion of $BNP_{O\text{-}C}$ to $BNP_{O\text{-}O}$ with associated rate constant k_{23}. These results support that $BNP_{C\text{-}C}$ is effectively converted directly to $BNP_{O\text{-}O}$.

IX. References

(1) Zhao, W.; Carreira, E. M. Facile One-Pot Synthesis of Photochromic Pyrans. *Org. Lett.* **2003**, *5*, 4153-4154.

(2) Beyer, M. K. The Mechanical Strength of a Covalent Bond Calculated by Density Functional Theory. *J. Chem. Phys.* **2000**, *112*, 7307–7312.

(3) Kryger, M. J.; Munaretto, A. M.; Moore, J. S. Structure-Mechanochemical Activity Relationships for Cyclobutane Mechanophores. *J. Am. Chem. Soc* **2011**, *133*, 18992–18998.

(4) Robb, M. J.; Kim, T. A.; Halmes, A. J.; White, S. R.; Sottos, N. R.; Moore, J. S. Regioisomer-Specific Mechanochromism of Naphthopyran in Polymeric Materials. *J. Am. Chem. Soc.* **2016**, *138*, 12328–12331.

(5) May, P. A.; Munaretto, N. F.; Hamoy, M. B.; Robb, M. J.; Moore, J. S. Is Molecular Weight or Degree of Polymerization a Better Descriptor of Ultrasound-Induced Mechanochemical Transduction? *ACS Macro Lett.* **2016**, *5*, 177–180.

(6) Berkowski, K. L.; Potisek, S. L.; Hickenboth, C. R.; Moore, J. S. Ultrasound-Induced Site-Specific Cleavage of Azo-Functionalized Poly(Ethylene Glycol). *Macromolecules* **2005**, *38*, 8975–8978.

(7) Li, J.; Nagamani, C.; Moore, J. S. Polymer Mechanochemistry: From Destructive to Productive. *Acc. Chem. Res.* **2015**, *48*, 2181–2190.

(8) Lu, X.; Dong, Q.; Dong, X.; Zhao, W. Synthesis and Sequential Photochromism of Thiophene-Linked Bis-Pyrans. *Tetrahedron* **2015**, *71*, 4061–4069.

(9) Zhao, W.; Carreira, E. M. Oligothiophene-Linked Bisnaphthopyrans: Sequential and Temperature-Dependent Photochromism. *Chem. Eur. J.* **2007**, *13*, 2671–2688.

(10) Odell, J. A.; Keller, A. Flow-Induced Chain Fracture of Isolated Linear Macromolecules in Solution. *J. Polym. Sci., Part B: Polym. Phys.* **1986**, *24*, 1889–1916.

(11) Wolfram Research, Inc. Mathematica. *Version 12.0*, **2019**.

(12) Collum, D. B. Numerical Integration – Simulation of Chemical Kinetics Using Mathematica 6.0, 2008. Collum Group Website (Cornell University): Simulation of Chemical Kinetics in Mathematica. http://collum.chem.cornell.edu/dbc6/Group_Resources.html (accessed June 15, 2019).

(13) Akbulatov, S.; Boulatov, R. Experimental Polymer Mechanochemistry and Its Interpretational Frameworks. *Chem. Phys. Chem.* **2017**, *18*, 1422–1450.

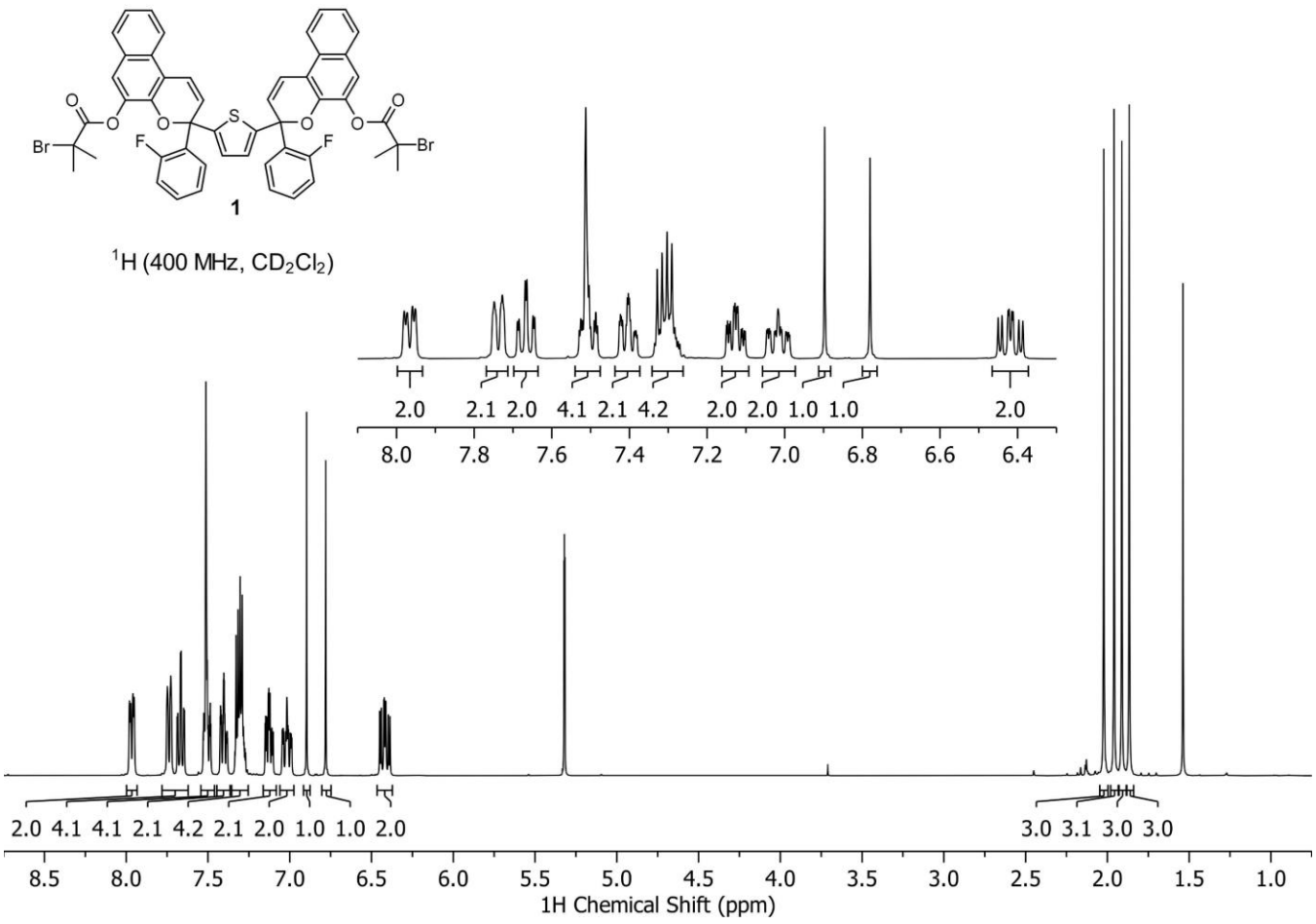
1
^{1}H (400 MHz, CD_2Cl_2)
2.0 2.1 2.0 4.1 2.1 4.2 2.0 2.0 1.0 1.0 2.0
8.0 7.8 7.6 7.4 7.2 7.0 6.8 6.6 6.4
2.0 4.1 4.1 2.1 4.2 2.1 2.0 1.0 1.0 2.0
3.0 3.1 3.0 3.0
8.5 8.0 7.5 7.0 6.5 6.0 5.5 5.0 4.5 4.0 3.5 3.0 2.5 2.0 1.5 1.0
1H Chemical Shift (ppm)

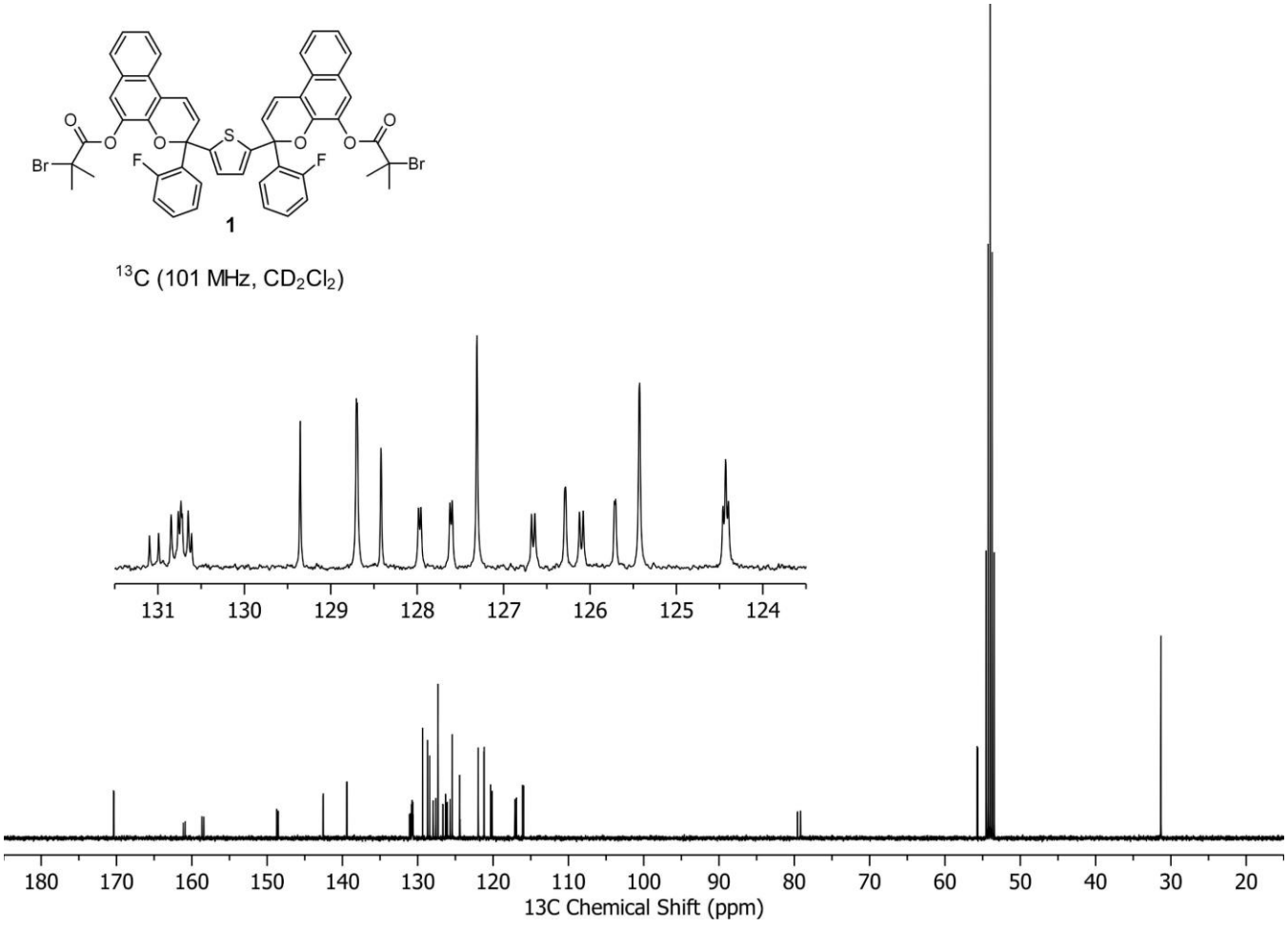
1
^{13}C (101 MHz, CD_2Cl_2)
131 130 129 128 127 126 125 124
180 170 160 150 140 130 120 110 100 90 80 70 60 50 40 30 20
13C Chemical Shift (ppm)

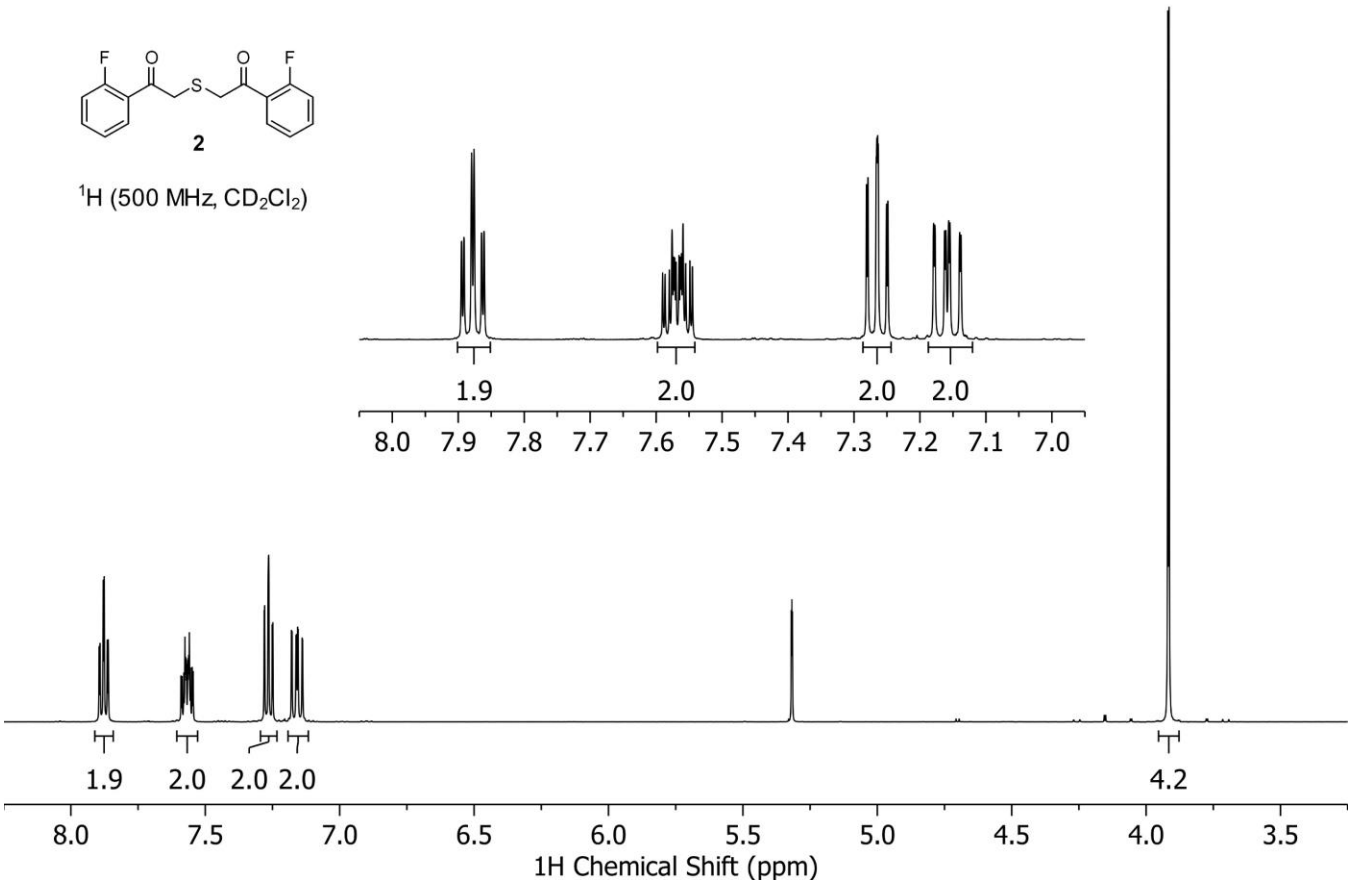
F
O
S
O
F
2
1H (500 MHz, CD2Cl2)
1.9
2.0
2.0
2.0
8.0
7.9
7.8
7.7
7.6
7.5
7.4
7.3
7.2
7.1
7.0
1.9
2.0
2.0
2.0
4.2
8.0
7.5
7.0
6.5
6.0
5.5
5.0
4.5
4.0
3.5
1H Chemical Shift (ppm)

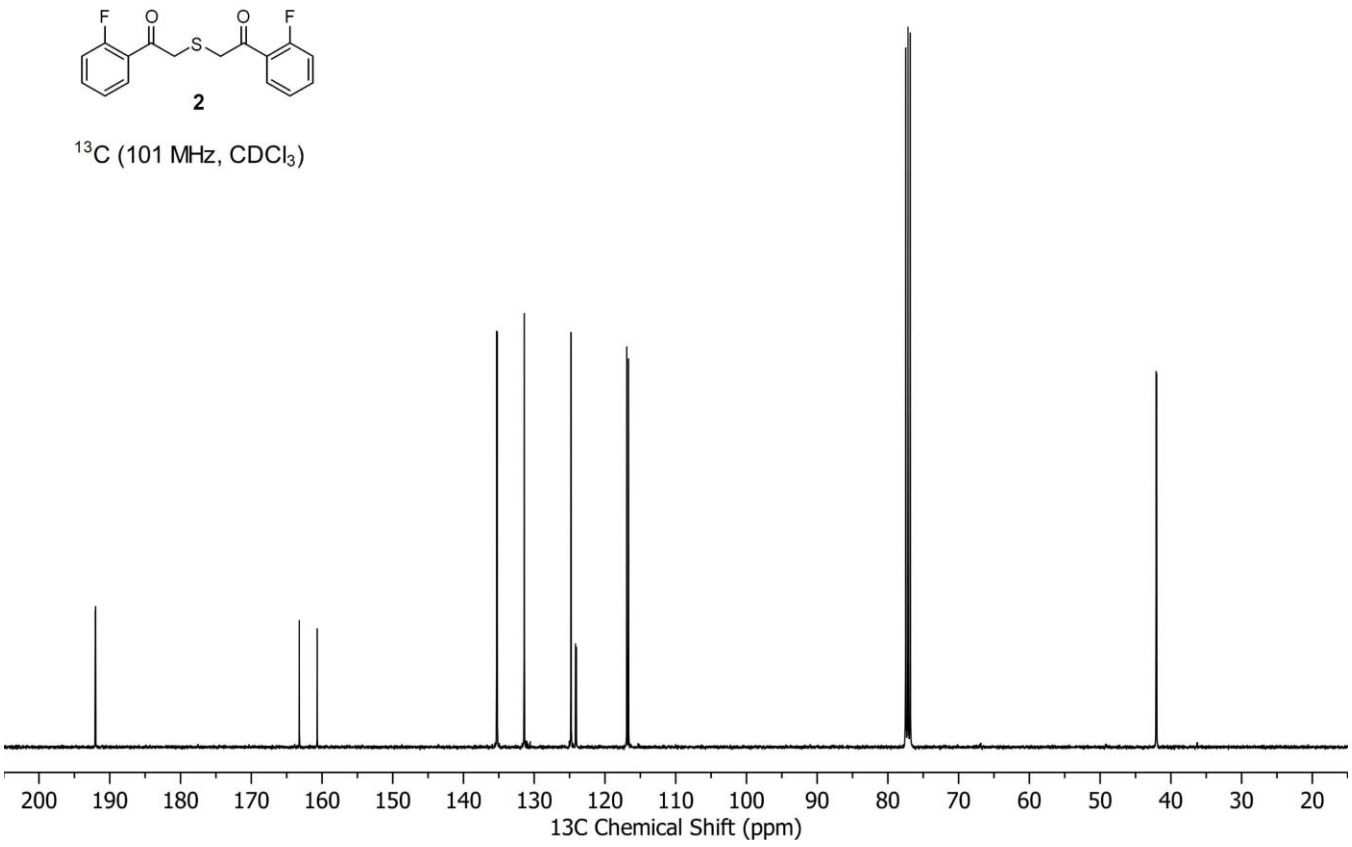
F
O
S
O
F
2
13C (101 MHz, CDCl3)
200
190
180
170
160
150
140
130
120
110
100
90
80
70
60
50
40
30
20
13C Chemical Shift (ppm)

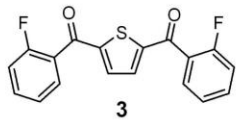

3

^{1}H (500 MHz, $CDCl_3$)

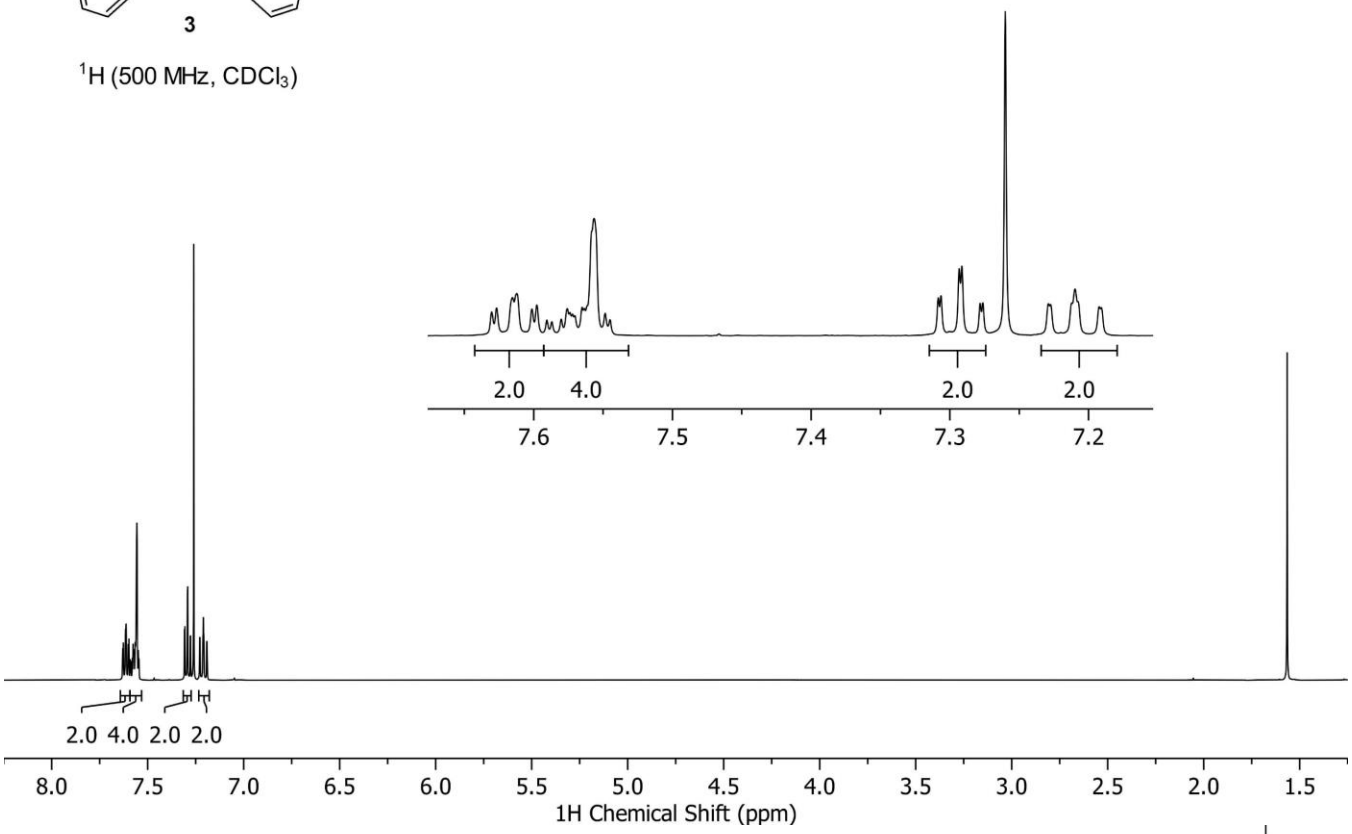

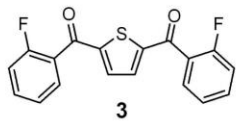

3

^{13}C (101 MHz, CD_2Cl_2)

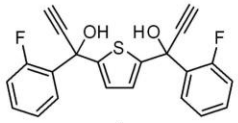

4

^{1}H (400 MHz, $CDCl_3$)

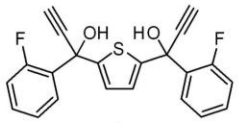

4

^{13}C (101 MHz, $CDCl_3$)

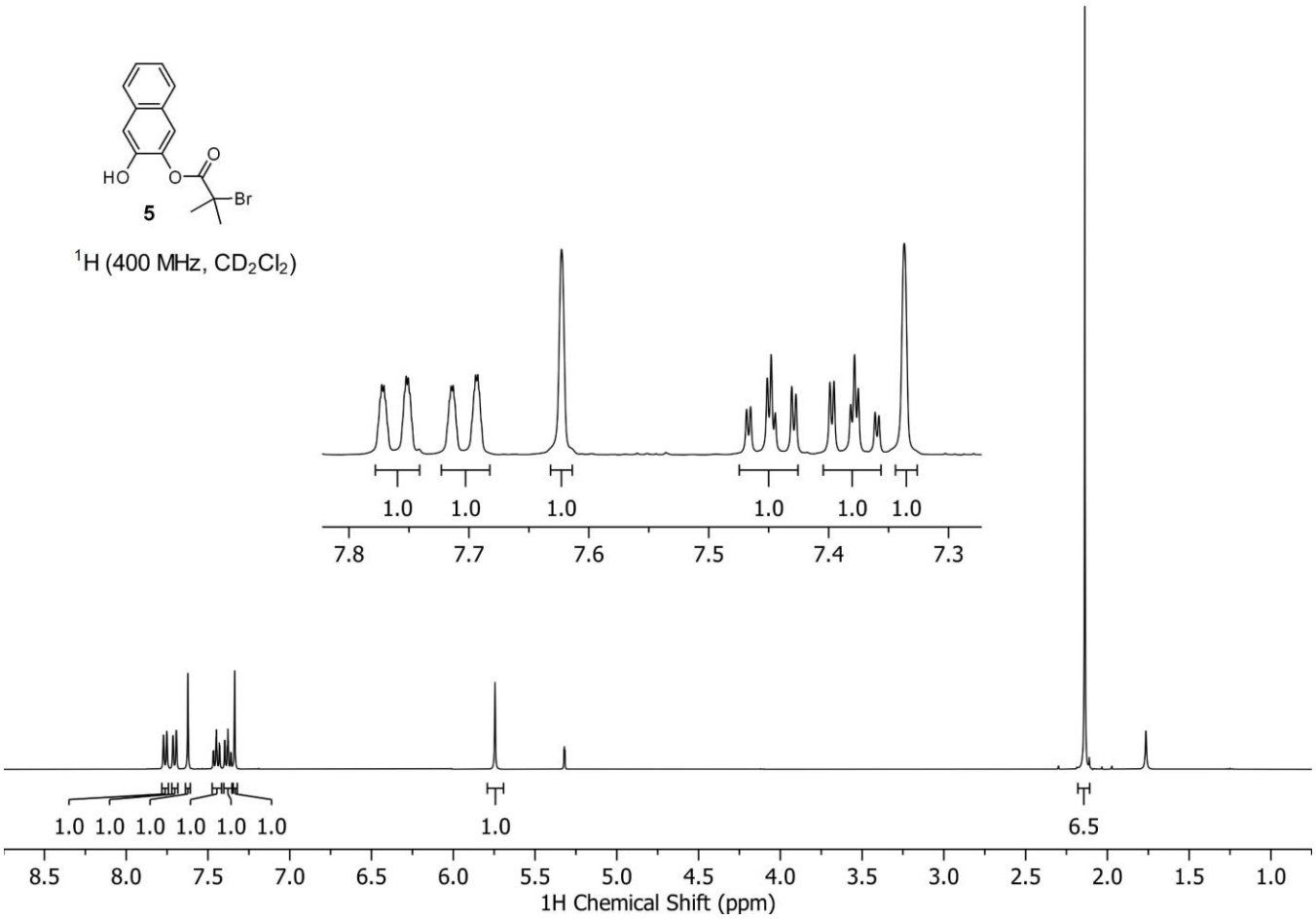
HO
O
O
Br
5
^{1}H (400 MHz, CD_2Cl_2)
1.0 1.0 1.0 1.0 1.0 1.0
7.8 7.7 7.6 7.5 7.4 7.3
1.0 1.0 1.0 1.0 1.0 1.0
1.0
6.5
8.5 8.0 7.5 7.0 6.5 6.0 5.5 5.0 4.5 4.0 3.5 3.0 2.5 2.0 1.5 1.0
1H Chemical Shift (ppm)

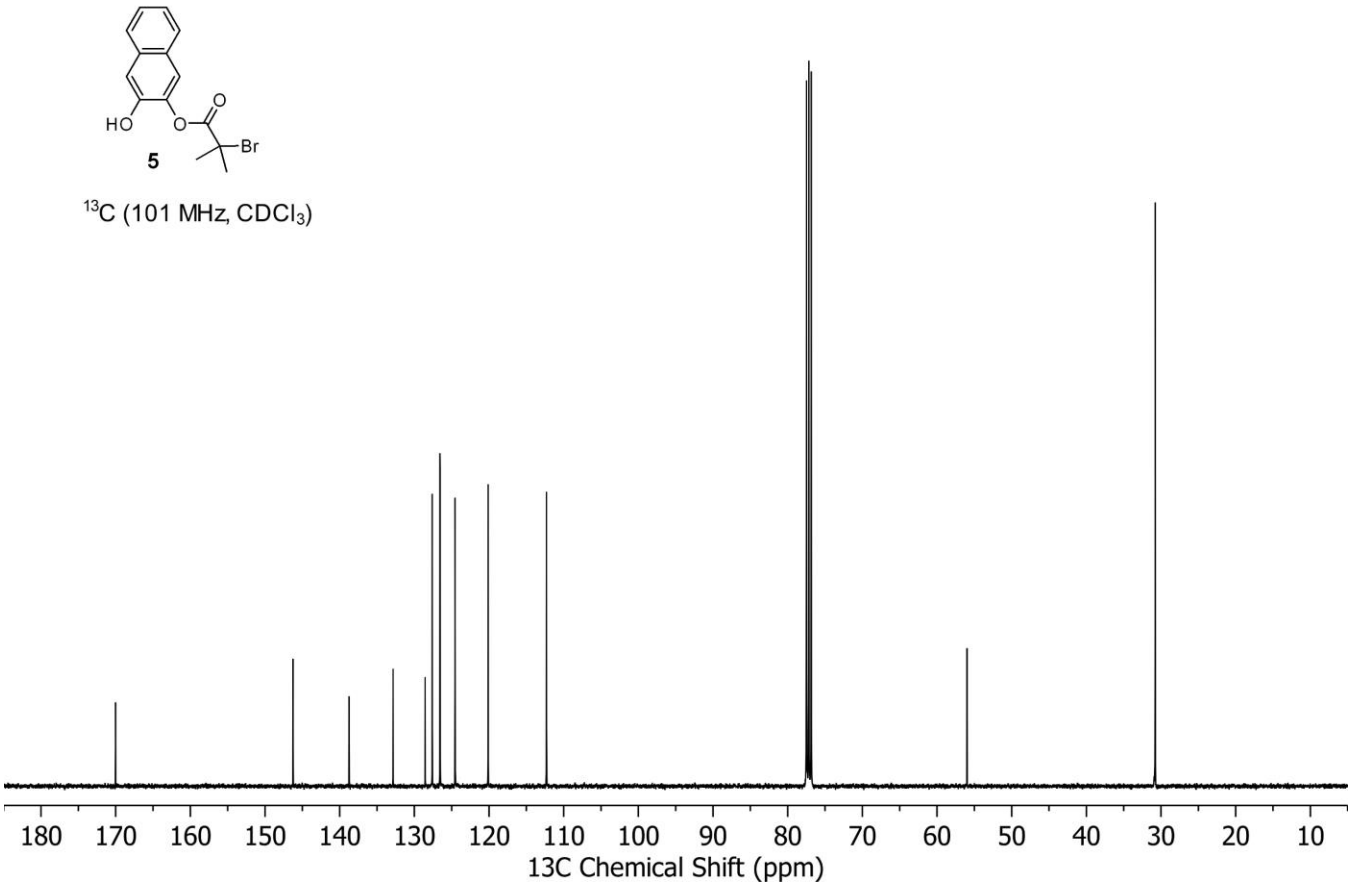
HO
O
O
Br
5
^{13}C (101 MHz, $CDCl_3$)
180 170 160 150 140 130 120 110 100 90 80 70 60 50 40 30 20 10
13C Chemical Shift (ppm)

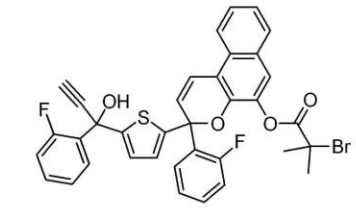

6

^{1}H (400 MHz, CD_2Cl_2)

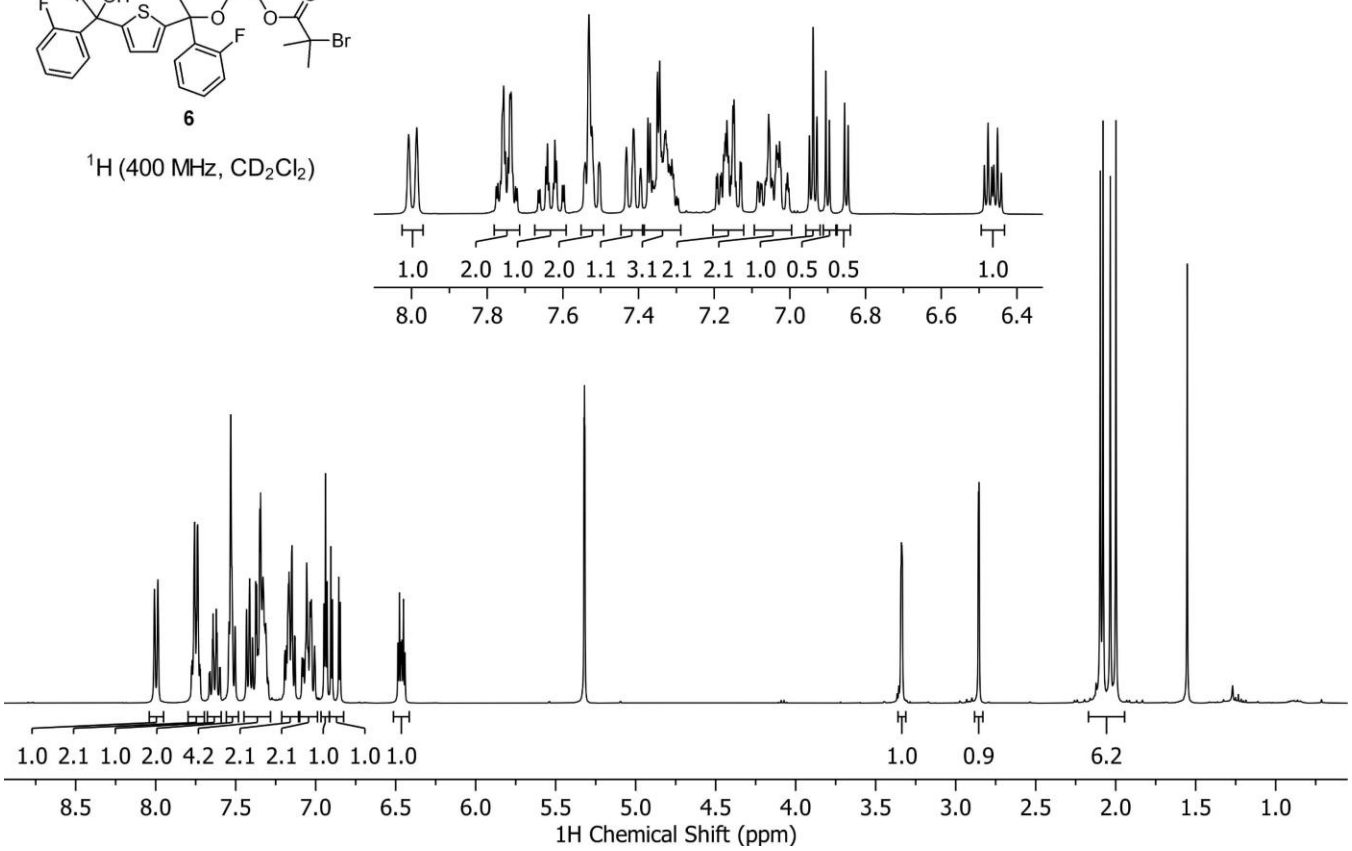

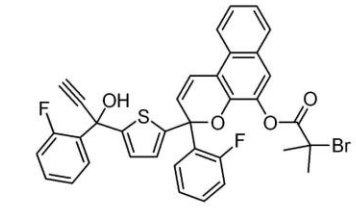

6

^{13}C (151 MHz, CD_2Cl_2)

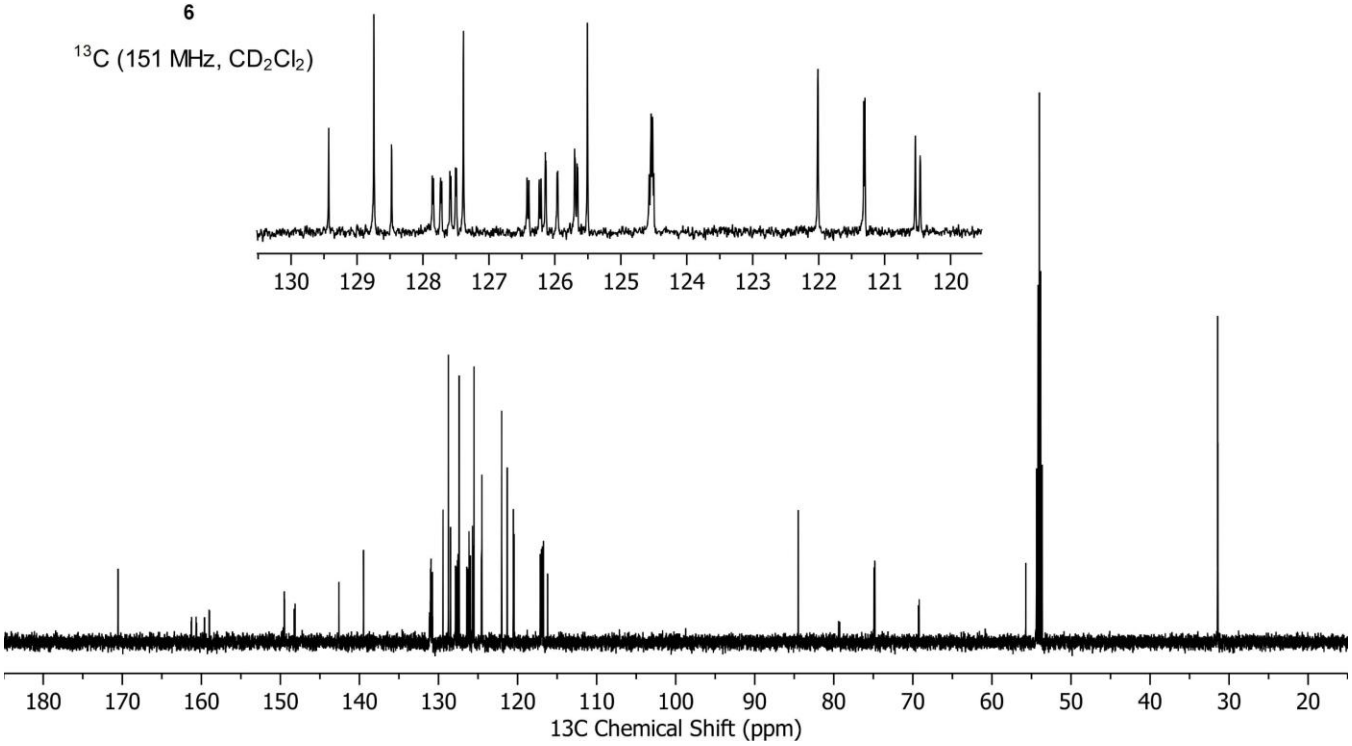

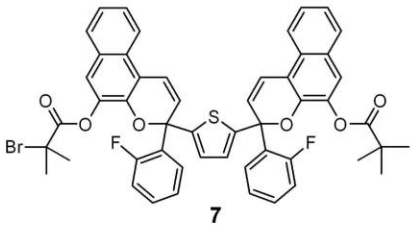

7

^{1}H (400 MHz, CD_2Cl_2)

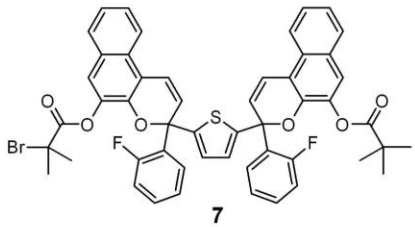

7

^{13}C (101 MHz, CD_2Cl_2)

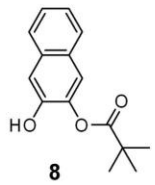

8

^{1}H (400 MHz, CD_2Cl_2)

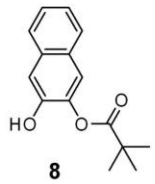

8

^{13}C (101 MHz, $CDCl_3$)